Supporting Information

Synthesis of a Rhenium(VII) Trioxo Complex Supported by a Triphyrin Ligand: Oxygenation Chemistry and Deposition on Au(111)

Manh Linh Nguyen,[a] Thomas Strunskus,[b] Christian Näther,[a] Jan Krahmer,[a] and Felix Tuczek*[a]

[a] Institute of Inorganic Chemistry, Christian Albrechts University Kiel, Germany

[b] Department of Material Science, Christian Albrechts University Kiel, Germany

Table of Contents

1. Instrumentation and Physical Methods

General Synthetic Procedures

Reactions under inert atmosphere were performed using standard Schlenk techniques. Most reagents and solvents were purchased from commercial sources and were used as received. Abs. solvents were dried over $LiAlH_4$ (THF) or CaH_2 (toluene) and freshly destilled under argon atmosphere prior to use. Air- and moisture-sensitive reagents were stored under nitrogen atmosphere in a M. Braun Labmaster 130 Glovebox.

Column Chromatography

Column chromatography for the purification of crude products was performed using silica gel 60 (0.04-0.063 mm) and ALOX 90 (neutral, activity 1) by Merck. Analytical thin layer chromatography (TLC) was carried out by using POLYGRAM SIL G/UV254 by Macherey-Nagel under UV light (lambda = 254 nm).

NMR Spectroscopy

NMR spectra were measured on Bruker (AVANCE^{TM} III HD Pulse FT) and Bruker (DRX 500) spectrometers. The chemical shifts are denoted in parts per million (ppm) and are referenced to the residual solvent peak of $CDCl_3$ (^1H = 7.26 ppm, ^{13}C = 77.16 ppm). The splitting parameters are denoted as follows: s (singlet), d (doublet), t (triplet), q (quartet), m (multiplet). In the analysis of the ^{13}C NMR spectra, primary, secondary, tertiary, and quaternary carbon atoms are denoted by the abbreviations C_p, C_s, C_t, and C_q, respectively.

UV/Vis Spectroscopy

UV/Vis measurements at room temperature were carried out using an Agilent 8453 spectrometer. Quartz cuvettes with a length of 1 cm were used for this purpose.

IR Spectroscopy

IR spectra were recorded on a Bruker Alpha FT-IR spectrometer with a Platinum ATR module in a range of 4000-400 cm^{-1} with a resolution of 4 cm^{-1}. Signal intensities are abbreviated as follows: w (weak), m (medium), s (strong), br. (broad).

Mass Spectrometer

High-resolution electrospray ionization spectrometry (HR-ESI) was performed on a Q Exactive™ Plus ESI-TOF mass spectrometer.

Elemental Analysis

Elemental analyses were performed using a Vario MICRO cube elemental analyzer (Elementar). Samples were prepared in tin capsules and combusted in an oxygen stream.

Gold Substrate

Glass substrates coated with a 50 Å titanium adhesion layer and a 200 nm evaporated gold film (EMF Corporation, Ithaca, NY) were used for IRRAS measurements. XPS and NEXAFS experiments were performed on sputter-cleaned Au(111) single crystals. Prior to each sample preparation, the gold-coated wafers and single crystals were cleaned by flame annealing in butane gas.

Preparation of Monolayers

Monolayers of compound **2** or **3** were prepared by immersing Au(111) substrates in 0.5 mM solution of **2** or **3** in dichloromethane at room temperature. The substrates were left in solution for 60 minutes, then removed, rinsed with DCM to eliminate unbound species, and dried under a stream of nitrogen gas.

Surface Characterization Methods

Infrared Reflection Absorption Spectroscopy (IRRAS) measurements were conducted using a Bruker VERTEX 70 FT-IR spectrometer equipped with a Polarization Modulation Accessory (PMA 50 unit, Bruker Optik GmbH, Ettlingen, Germany). This setup allowed for the acquisition of both IRRAS and PM-IRRAS spectra within the spectral range of 4000 to 750 cm^{-1}. IRRAS data were collected using a liquid nitrogen-cooled MCT detector in a horizontal reflection unit (Bruker A518) under grazing incidence geometry. The sample chamber was purged with dry nitrogen before and during measurements to minimize atmospheric interference. For background correction, an undeuterated hexadecane-thiol self-assembled monolayer (SAM) on Au(111) was used as the reference. Each spectrum consisted of an average of 2048 scans, recorded with a p-polarized beam incident at an angle of 80° relative to the

surface normal. Spectra were collected with a resolution of 4 cm^{-1}. For PM-IRRAS, the PMA 50 accessory was used in conjunction with the liquid nitrogen-cooled MCT detector. The polarizer was set to maximize efficiency at the half-wave of 1750 cm^{-1}, covering the spectral range from 2000 to 1000 cm^{-1}. PM-IRRAS spectra were recorded with a resolution of 4 cm^{-1}. Data processing for both IRRAS and PM-IRRAS was carried out using OPUS software (Version 6.5, Bruker, Germany). Baseline correction for the IRRAS spectra was performed using the rubber band method in interactive mode. For PM-IRRAS, baseline correction was carried out manually, with implicit removal of the Bessel function.

X-ray Photoelectron Spectroscopy (XPS) measurements were conducted at the BESSY II synchrotron radiation facility at the HE-SGM beamline. The experimental station was equipped with a hemispherical VG Scienta R3000 photoelectron analyzer. The beamline energy resolution (E/ΔE) with 150 mm slits was set to 800. XP survey spectra were acquired at a photon energy of 700 eV, with an analyzer pass energy of 100 eV. For the C 1s and Re 4f spectra, a photon energy of 350 eV and pass energy of 50 eV were used, while the N 1s spectra were recorded at 500 eV photon energy and 50 eV pass energy. The O 1s spectra were measured at 650 eV photon energy and 50 eV pass energy. All spectra were recorded with normal electron emission. For relative composition determination, XPS spectra were energy-corrected using the Au $4f_7/_2$ line at a binding energy of 84.0 eV as the reference. Background correction was performed using a combination of Shirley and linear background subtraction for all spectral signals. Peak fitting was performed using the CASA XPS software. For the NEXAFS measurements, all spectra were divided by the corresponding spectrum of a freshly sputtered clean gold substrate and then edge-step normalized. The normalization was performed using the average pre- and post-edge intensities for the C K-edge in the ranges 275 ± 0.5 eV and 320 ± 0.5 eV, respectively, and for the N K-edge in the ranges 395 ± 0.5 eV and 420 ± 0.5 eV.

Computational Methods

Preliminary geometry optimizations were performed using Avogadro[1] with the Universal Force Field (UFF).[2] The final geometry optimizations, along with density functional theory (DFT) energy and frequency calculations, were carried out using ORCA 4.2.1.[3] The hybrid density functional approximation B3LYP[4] was employed, in combination with the def2-SVP basis set[5] and the D3 dispersion correction with Becke–

Johnson damping (D3BJ).[6,7] The RIJCOSX approximation[8] was applied in combination with the def2 fitting basis set (def2/J)[4,9] and fine numerical integration grids (grid4 and gridX4 in ORCA nomenclature) were used to ensure accuracy and efficiency in the calculations.

Single Crystal Structure Determination

The data collections were performed with a XtaLAB Synergy, Dualflex, HyPix diffractometer with a micro focus tube using Cu-Kα radiation (λ = 1.54184 Å). The structures were solved with SHELXT[10] and refined with SHELXL[11] using Least Squares minimisation. All non-hydrogen atoms were refined anisotropic. The C-H H atoms were positioned with idealized geometry, methyl H atoms allowed to rotate but not to tip, and were refined isotropic with $U_{iso}(H) = 1.2\ U_{eq}(C)$ (1.5 for methyl H atoms) using a riding model. After structure refinement of **3** there are some residual electron density peaks, indicating for disordered solvent. Because no reasonable structure model was found its contribution to the electron density map was removed.

CCDC-2530155 (**2**), CCDC-2530156 (**3**), and CCDC-2530157 (**3-Et$_2$O**) contain the supplementary crystallographic data for this paper. These data can be obtained free charge from the Cambridge Crystallographic Data Centre via http://www.ccdc.cam.ac.uk/data_request/cif.

2. Experimental Section

2.1 Synthesis of Benzyl-3,5-dimethyl-4-ethylpyrrole-2-carboxylate (4)

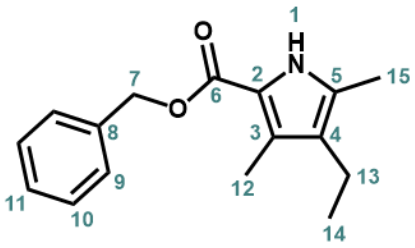

The synthesis was performed according to the procedure reported by Uno *et al.*[12] A solution of benzylacetoacetate (5.38 g, 28.0 mmol) in acetic acid (5.6 mL) was treated dropwise at 0 °C over 1 h with a solution of sodium nitrite (1.98 g, 29.0 mmol) in deionized water (6.8 mL). The reaction mixture was stirred at room temperature for 18 h. The resulting orange solution was then added dropwise without further purification to a solution of 3-*n*-ethylpentane-2,4-dione (1.03 g, 8.00 mmol) in acetic acid (5.6 mL), zinc powder (2.71 g, 41.4 mmol) and sodium acetate (3.40 g, 41.4 mmol) at 80 °C. The mixture was then stirred at 93 °C for 2 h, after which the reaction mixture was quenched with ice (60 mL). The resulting solid was collected by filtration and purified by column chromatography (silica gel; cyclohexane/ethylacetate, 3:7; R_F: 0.53) obtaining a light yellow solid (1.32 g, 5.12 mmol, 64 %).

^{1}H-NMR (600 MHz, $CDCl_3$, 300 K): δ = 8.76 (s, 1H, -N*H*), 7.45 – 7.30 (m, 5H, *H*-9, *H*-10, *H*-11), 5.31 (s, 2H, *H*-7), 2.39 (q, *J* = 7.6 Hz, 2H, *H*-13), 2.31 (s, 3H, *H*-15), 2.20 (s, 3H, *H*-12), 1.06 (t, *J* = 7.6 Hz, 3H, *H*-14) ppm.

^{13}C-NMR (151 MHz, $CDCl_3$, 300 K): δ = 161.52 (C_q, *C*-6), 136.84 (C_q, *C*-8), 129.72 (C_q, *C*-3), 128.63 (C_t, *C*-10), 128.15 (C_t, *C*-9), 128.10 (C_t, *C*-11), 127.54 (C_q, *C*-5), 124.14 (C_q, *C*-4), 116.43 (C_q, *C*-2), 65.48 (C_d, *C*-7), 17.32 (C_s, *C*-13), 15.44 (C_p, *C*-14), 11.47 (C_p, *C*-12), 10.69 (C_p, *C*-15) ppm.

HRMS (ESI, 70 eV): *m/z calcd for $C_{16}H_{20}NO_2$: 258.15 $[M+H]^+$; Found: 258.15.*

Elemental Analysis:

$C_{16}H_{19}NO_2$	C [%]	N [%]	H [%]
calculated	74.68	5.44	7.44
found	74.12	5.40	7.63

IR: $\tilde{\nu}$ = 3305 (s, br), 3069 (w), 3033 (w), 2966 (m), 2924 (m), 2861 (m), 1746 (m), 1653 (s, br), 1500 (m), 1434 (s), 1377 (w), 1318 (w), 1267 (s), 1254 (s), 1215 (m), 1168 (m), 1117 (s), 1082 (m), 1028 (m), 993 (m), 961 (w), 909 (w), 880 (w), 817 (w), 771 (s), 745 (m), 733 (m), 692 (s), 621 (m), 595 (w), 571 (w), 494 (w), 439 (w), 405 (w), 376 (w), 302 (w), 263 (m), 216 (w), 151 (w) cm^{-1}.

2.2 Synthesis of Benzyl-5-acetoxy-4-ethyl-3-methylpyrrole-2-carboxylate (5)

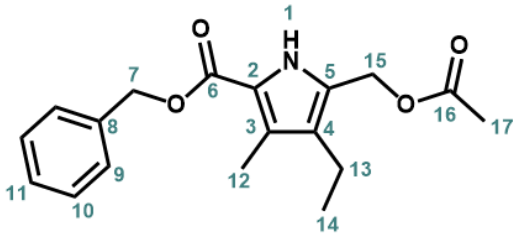

The synthesis was performed with modifications according to the procedure reported by Uno *et al.*[12] A solution of **4** (1.32 g, 5.12 mmol) in acetic acid (40 mL) and acetic anhydride (1.0 mL) was treated at room temperature with lead(IV)acetate (2.66 g, 6.0 mmol) over 5 min. The reaction mixture was stirred at room temperature for 2 h, then cooled deionized water (50 mL) was added. The resulting precipitate was collected by filtration and washed with a small amount of deionized water. The off-white solid was dissolved in chloroform (80 mL), washed with deionized water (30 mL), and dried over sodium sulfate. The solvent was removed under reduced pressure, and the residue was triturated with ethanol to give a light yellow solid (1.29 g, 4.10 mmol, 80 %).

^{1}H-NMR (500 MHz, $CDCl_3$, 300 K): δ = 9.02 (s, 1H, -N*H*), 7.45 – 7.30 (m, 5H, *H*-9, *H*-10, *H*-11), 5.31 (s, 2H, *H*-7), 5.01 (s, 2H, *H*-15), 2.46 (q, *J* = 7.6 Hz, 2H,*H*-13), 2.29 (s, 3H, *H*-12), 2.06 (s, 3H, *H*-17), 1.08 (t, *J* = 7.6 Hz, 3H, *H*-14) ppm.

^{13}C-NMR (151 MHz, $CDCl_3$, 300 K): δ = 171.66 (C_q, *C*-16), 161.28 (C_q, *C*-2), 136.51 (C_q, *C*-8), 128.69 (C_t, *C*-9), 128.27 (C_t, *C*-10, *C*-11), 127.14 (C_q, *C*-5), 126.94 (C_q, *C*-3), 126.66 (C_q, *C*-4), 119.04 (C_q, *C*-2), 65.83 (C_s, *C*-7), 57.07 (C_s, *C*-15), 21.08 (C_s, *C*-13), 17.22 (C_p, *C*-17), 16.09 (C_p, *C*-14), 10.46 (C_p, *C*-12) ppm.

HRMS (ESI, 70 eV): *m/z calcd for $C_{18}H_{22}NO_4$: 316.16 $[M+H]^+$; Found: 316.16*

Elemental Analysis:

$C_{18}H_{21}NO_4$	C [%]	N [%]	H [%]
calculated	68.55	4.44	6.71
found	68.51	4.46	6.63

IR: $\tilde{\nu}$ = 3310 (s), 3067 (w), 3039 (w), 2953 (m), 2926 (m), 2865 (m), 1732 (s), 1664 (s), 1587 (w), 1577 (w), 1501 (w), 1469 (m), 1447 (m), 1379 (s), 1355 (m), 1281 (s), 1258 (m), 1234 (m), 1209 (m), 1171 (m), 1120 (s), 1082 (m), 1021 (m), 989 (m), 954 (m), 914 (m), 889 (w), 849 (m), 774 (m), 747 (m), 697 (s), 599 (m), 576 (w), 503 (m), 481 (m), 429 (w) cm^{-1}.

2.3 Synthesis of 2,5-Bis[[5-(benzyloxycarbonyl)-3-ethyl-4-methylpyrrole-2-yl]methyl]-3,4-diethylpyrrole (6)

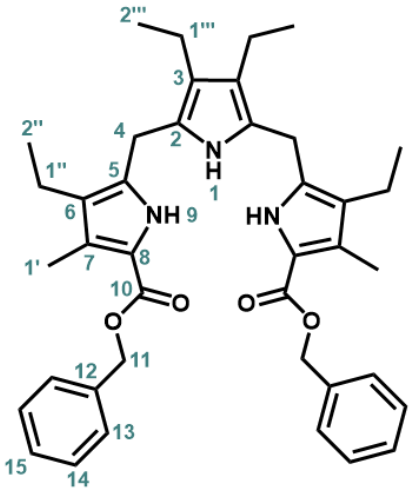

Following the procedure reported by Uno *et al.*[12] Compound **5** (1.29 g, 4.10 mmol) and 3,4-diethylpyrrole (253 mg, 2.05 mmol) were added to a solution of ethanol (25 mL) and acetic acid (2 mL). The reaction mixture was stirred at 82 °C in the dark for 18 h. After cooling to room temperature, the solution was stored at -18 °C overnight. The precipitated solid was collected by filtration and washed with cold ethanol, affording an off-white solid (1.00 g, 1.60 mmol, 78 %).

^{1}H-NMR (400 MHz, $CDCl_3$, 300 K): δ = 11.10 (s, 2H, *H*-9), 8.75 (s, 1H, *H*-1), 7.56 – 7.13 (m, 10H, *H*-13, *H*-14), 7.07 – 6.94 (m, 4H, *H*-15), 4.43 (s, 4H, *H*-11), 3.55 (s, 4H, *H*-4), 2.54 (q, ^3J = 7.5 Hz, 4H, *H*-1‘), 2.42 – 2.32 (m, 4H, *H*-1‘‘), 2.29 (s, 6H, *H*-1‘), 1.19 (t, ^3J = 7.5 Hz, 6H, *H*-2‘‘’), 1.01 (t, ^3J = 7.5 Hz, 6H, *H*-2‘‘) ppm.

^{13}C-NMR (101 MHz, $CDCl_3$, 300 K): δ = 162.68 (C_q, *C*-10), 137.17 (C_q, *C*-12), 133.09 (C_q, *C*-8), 128.20 (C_t, *C*-13), 127.25 (C_t, *C*-14), 126.60 (C_t, *C*-15), 123.11 (C_q, *C*-3), 122.52 (C_q, *C*-6), 118.87 (C_q, *C*-2), 117.28 (C_q, *C*-5), 65.35 (C_s, *C*-11), 22.15 (C_s, *C*-4), 17.91 (C_s, *C*-1'''), 17.36 (C_s, *C*-1''), 17.04 (C_p, *C*-2'''), 15.94 (C_p, *C*-2''), 11.15 (C_p, *C*-1') ppm.

HRMS (ESI, 70 eV): *m/z calcd for $C_{40}H_{48}N_3O_4$: 634.34 [M+H]$^+$; Found: 634.34.*

Elemental Analysis:

$C_{40}H_{47}N_3O_4$	C [%]	N [%]	H [%]
calculated	75.80	6.63	7.47
found	73.44	6.17	7.47

IR: $\tilde{\nu}$ = 3413 (m), 3289 (s), 3091 (w), 3066 (w), 3034 (w), 2960 (s), 2927 (s), 2867 (s), 1731 (w), 1651 (s), 1586 (w), 1498 (m), 1448 (s), 1419 (m), 1372 (w), 1300 (m), 1277 (s), 1256 (s), 1223 (m), 1175 (w), 1149 (m), 1118 (m), 1085 (m), 1062 (m), 1031 (w), 988 (m), 961 (m), 920 (w), 888 (w), 768 (m), 726 (s), 693 (s), 635 (m), 593 (w), 567 (w), 528 (w), 478 (w), 451 (m), 384 (w), 337 (w), 299 (w), 257 (w) cm^{-1}.

2.4 Synthesis of 2,5-Bis[[5-(formyl)-3-ethyl-4-methylpyrrole-2-yl]methyl]-3,4-diethylpyrrole (7)

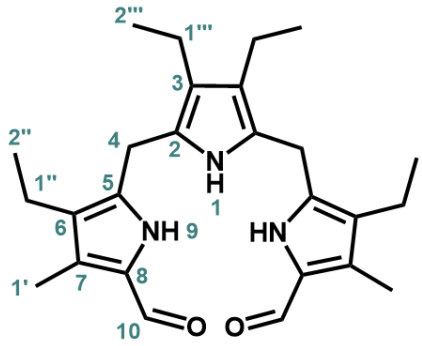

The synthesis was performed according to the procedure reported by Uno *et al.* The synthesis was performed under a hydrogen atmosphere with inert gas protection. Under nitrogen, Pd/C (10 %, 100 mg) was suspended in anhydrous THF (10 mL). The reaction vessel was evacuated and refilled with H_2 gas three times. A solution of compound **6** (1.00 g, 1.60 mmol) in anhydrous THF (20 mL) containing one drop of triethylamine (TEA) was then added to the suspension. The mixture was stirred

overnight at room temperature under a hydrogen atmosphere. The reaction mixture was filtered through Celite and washed with ethyl acetate (40 mL). The solvent was removed under reduced pressure to give a red-white solid. Under nitrogen, trifluoroacetic acid (2.8 mL) was added at 0 °C to the above mentioned, obtained solid. Subsequently, trimethyl orthoformate (5.5 mL) was added dropwise over 10 min at 0 °C. The mixture was stirred for 1 h at 0 °C, followed by the neutralization with 40 mL of 1 M NaOH in 50 % aqueous methanol. The reaction mixture was poured into cooled deionized water (110 mL). The precipitate was collected by filtration, washed with water and *n*-hexane, affording a light purple solid (594 mg, 1.41 mmol, 97 %).

^{1}H-NMR (400 MHz, $CDCl_3$, 300 K): δ = 10.19 (s, 2H, *H*-9), 9.35 (s, 1H, *H*-1), 9.01 (s, 2H, *H*-10), 3.82 (s, 4H, *H*-4), 2.41 (m, 8H, *H*-1'', *H*-1'''), 2.14 (s, 6H, *H*-1'), 1.09 (t, ^{3}J = 7.5 Hz, 6H, *H*-2'''), 1.01 (t, ^{3}J = 7.5 Hz, 6H, *H*-2'') ppm.

^{13}C-NMR (101 MHz, $CDCl_3$, 300 K): δ = 175.71 (C_t, *C*-10), 138.10 (C_q, *C*-5), 133.12 (C_q, *C*-8), 128.17 (C_q, *C*-7), 124.68 (C_q, *C*-2), 121.63 (C_q, *C*-6), 120.84 (C_q, *C*-3), 22.72 (C_s, *C*-4), 17.81 (C_s, *C*-1'''), 17.10 (C_s, *C*-1''), 16.71 (C_p, *C*-2'''), 15.37 (C_s, *C*-2''), 8.85 (C_s, *C*-1') ppm.

HRMS (ESI, 70 eV): *m/z calcd for $C_{26}H_{37}N_3O_2$:* 422.28 *$[M+H]^+$; Found:* 422.28.

Elemental Analysis:

$C_{26}H_{35}N_3O_2$	C [%]	N [%]	H [%]
calculated	74.07	9.97	8.37
found	73.61	9.77	8.07

IR: $\tilde{\nu}$ = 3278 (s, br), 3200 (s), 3076 (w), 2960 (s), 2926 (m), 2866 (m), 2843 (m), 1634 (s, br), 1445 (s), 1378 (m), 1341 (m), 1319 (w), 1296 (w), 1271 (m), 1203 (w), 1193 (w), 1144 (m), 1101 (w), 1062 (m), 979 (w), 959 (w), 897 (w), 868 (m), 853 (w), 781 (s), 736 (w), 697 (w), 673 (w), 641 (w), 575 (w), 535 (w), 496 (w), 432 (w), 397 (m), 386 (m), 303 (m), 264 (w), 204 (w), 153 (w) cm^{-1}.

2.5 Synthesis of 2,3,7,14-Tetraethyl 8,13-dimethyl[14]triphyrin(2.1.1) (TriP^{Et}, 1)

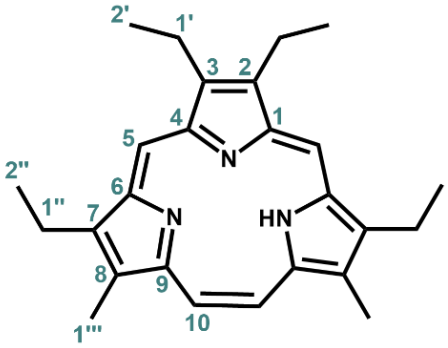

The synthesis was performed under nitrogen atmosphere. A suspension of CuCl (518 mg, 5.23 mmol) and Zn dust (3.50 g, 53.5 mmol) in abs. THF (100 mL) was cooled down to 0 °C. Then $TiCl_4$ (5.10 g, 26.9 mmol) was added slowly into the suspension and the mixture was then stirred for 2 h at 80 °C. Afterward, a solution of tripyrrane dicarbaldehyde (**7**, 461 mg, 1.09 mmol) in abs. THF (200 mL) was added dropwise over 120 min into the reaction mixture and the mixture was then stirred for 3 h under reflux. After the reaction, the mixture was quenched with 10 % aqueous K_2CO_3 (150 mL) at 0 °C. The resulting solid was filtered through Celite and the filter cake was washed with ethyl acetate. The combined organic layer was subsequently dried over Na_2SO_4 and the solvents were evaporated under reduced pressure at RT. The residue was purified by column chromatography (ALOX, $CHCl_3$) and DDQ (496 mg, 2.18 mmol) was added to the eluted solution. The mixture was then stirred overnight at RT. The resulting black solution was washed with brine and aqueous $NaHCO_3$ and dried over Na_2SO_4. The solvent was evaporated under reduced pressure and the crude product was purified by column chromatography (silica gel, $CHCl_3$/MeOH 85:15, R_f=0.52). The product was obtained as a red solid (118 mg, 33 µmol, 31 %).

^{1}H-NMR (500 MHz, $CDCl_3$): δ = 8.93 (s, 2H, *H*-10), 8.88 (s, 2H, *H*-5), 6.52 (s, 1H, -N*H*), 3.52 (q, ^3J = 7.7 Hz, 4H, *H*-1'), 3.25 (q, ^3J = 7.7 Hz, 4H, *H*-1''), 3.02 (s, 6H, *H*-1'''), 1.59 (t, ^3J = 7.7 Hz, *H*-2'), 1.53 (t, ^3J = 7.4 Hz, 6H, *H*-2'') ppm.

^{13}C-NMR (126 MHz, $CDCl_3$): δ = 157.10 (q, *C*-1,4), 152.85 (q, *C*-9,12), 145.66 (q, *C*-6,15), 143.98 (q, *C*-7,14), 139.83 (q, *C*-2,3), 133.95 (q, *C*-8,13), 115.30 (t, *C*-10,11), 108.13 (t, *C*-5,16), 19.42 (s, *C*-1'), 19.16 (s, *C*-1''), 17.60 (p, *C*-2''), 17.22 (p, *C*-2'), 10.66 (p, *C*-1''') ppm.

HRMS (ESI, 70 eV): *m/z calcd for $C_{26}H_{32}N_3$:* 386.26 *$[M+H]^+$; Found:* 386.26.

IR: $\tilde{\nu}$ = 2958 (s), 2925 (s), 2865 (s), 1705 (m), 1659 (m), 1567 (w), 1491 (w), 1461 (m), 1447 (m), 1373 (w), 1343 (w), 1312 (w), 1265 (w), 1256 (w), 1219 (w), 1205 (w), 1189 (w), 1158 (w), 1137 (w), 1126 (w), 1057 (m), 1011 (m), 947 (m), 886 (w), 848 (w), 810 (w), 800 (m), 754 (w), 728 (w), 682 (w), 616 (w), 566 (w), 500 (w), 455 (w), 423 (w), 363 (w), 300 (w), 275 (w) cm^{-1}.

Raman: $\tilde{\nu}$ = 3039 (w), 2966 (m), 2927 (m), 2867 (m), 1562 (m), 1540 (s), 1486 (m), 1453 (w), 1391 (m), 1357 (w), 1286 (s), 1269 (w), 1226 (m), 1211 (m), 1147 (w), 1137 (w), 1119 (w), 1061 (w), 1025 (w), 993 (w), 968 (w), 921 (m), 896 (w), 817 (w), 769 (w), 732 (w), 651 (w), 600 (w), 525 (w), 468 (w), 414 (w), 356 (m), 334 (w), 284 (w), 183 (w) cm^{-1}.

UV/Vis (CH_2Cl_2): λ_{max} (ε) = 247 (17300), 337 (79500), 514 (12350) 548 (10450) nm.

Elemental Analysis:

$C_{26}H_{31}N_3$	C [%]	N [%]	H [%]
calculated	81.00	10.90	8.10
found	75.31	10.05	7.77

2.6 Synthesis of [Re(TriP^{Et})(CO)$_3$] (2)

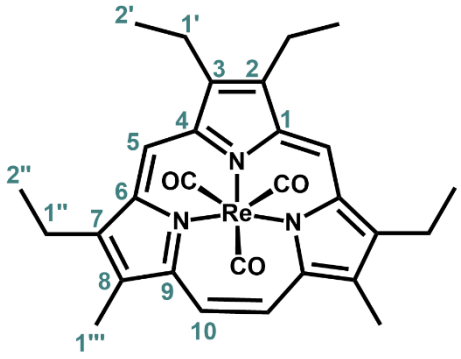

The synthesis was performed under nitrogen atmosphere. A mixture of TriP^{Et} (**1**, 40 mg, 104 µmol), [ReCl(CO)$_5$] (200 mg, 553 µmol) and NaOAc (94 mg, 1.15 mmol) in abs. toluene (10 mL) was stirred overnight at 110 °C. Afterwards the reaction mixture was allowed to cooldown to room temperature and the solvent was evaporated under reduced pressure. The crude product was purified by column chromatography (silica gel, $CHCl_3$, R_f=0.72) and was obtained as a dark red solid (62 mg, 95 µmol, 91 %).

^{1}H-NMR (400 MHz, $CDCl_3$): δ = 8.96 (s, 2H, *H*-10), 8.86 (s, 2H, *H*-5), 3.44 – 3.00 (m, 8H, *H*-1',1''), 2.72 (s, 6H, *H*-1'''), 1.47 (t, ^{3}J = 7.6 Hz, 6H, *H*-2'), 1.37 (t, ^{3}J = 7.7 Hz, 6H, *H*-2'') ppm.

^{13}C-NMR (101 MHz, $CDCl_3$): δ = 197.28 (q, *C*O), 194.68 (q, $(CO)_2$), 161.48 (q, *C*-1,4), 161.22 (q, *C*-9), 157.19 (q, *C*-6), 140.64 (q, *C*-7), 137.11 (q, *C*-2,3), 132.44 (q, *C*-8), 119.74 (t, *C*-10), 115.09 (t, *C*-5), 18.91 (s, *C*-1'), 18.68 (s, *C*-1''), 17.45 (p, *C*-2''), 16.63 (p, *C*-2'), 10.74 (p, *C*-1''') ppm.

HRMS (ESI, 70 eV): *m/z calcd for $C_{29}H_{31}N_3O_3Re$:* 654.19 *$[M+H]^+$; Found:* 654.19.

IR: $\tilde{\nu}$ = 2970 (m), 2931 (m), 2872 (m), 1996 (s), 1876 (s, br), 1865 (s, br), 1463 (m, br), 1452 (m, br), 1417 (w), 1383 (w), 1350 (w), 1314 (w), 1269 (w), 1238 (w), 1213 (w), 1187 (w), 1148 (m), 1133 (w), 1112 (w), 1091 (w), 1059 (m), 1020 (w), 1001 (w), 972 (w), 949 (w), 881 (m), 813 (m), 766 (w), 746 (w), 730 (w), 709 (w), 685 (w), 670 (w), 646 (m), 634 (m), 622 (m), 611 (m), 553 (w), 539 (m), 506 (w), 488 (m) cm^{-1}.

Raman: $\tilde{\nu}$ = 1889 (w), 1869 (w), 1559 (w), 1535 (s), 1487 (w), 1452 (w), 1414 (w), 1393 (w), 1376 (w), 1355 (w), 1278 (m), 1239 (w), 1214 (w), 1060 (w), 1021 (w), 992 (w), 965 (w), 898 (w), 872 (w), 827 (w), 769 (w), 724 (w), 645 (w), 600 (w), 503 (w), 465 (w), 394 (w), 362 (w), 326 (w), 281 (w) cm^{-1}.

UV/Vis (CH_2Cl_2): λ_{max} (ε) = 230 (16830), 269 (14190), 347 (38100), 468 (4949), 558 (3165) nm.

2.7 Synthesis of [ReO_3(TriP^{Et})] (3)

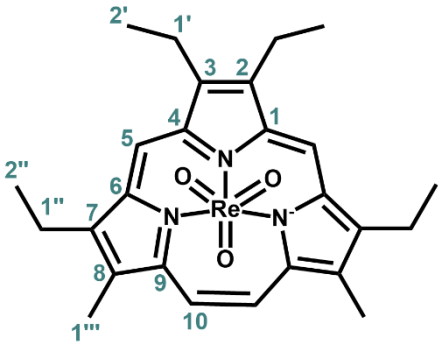

A mixture of [Re(TriP^{Et})$(CO)_3$] (**2**, 32 mg, 49 µmol) and 140 µL *tert*-Butyl hydroperoxide (7 M in H_2O, 20 eq.) in abs. toluene (5 mL) was stirred at room temperature. The conversion to **3** was monitored by thin-layer chromatography (TLC) until completion. After completion (3 days) the solvent of the reaction mixture was evaporated under

reduced pressure. The crude product was purified by column chromatography (silica gel, $CHCl_3$/acetone 99:1, R_f=0.18) and was obtained as a bright red solid (18 mg, 29 µmol, 59 %).

^{1}H-NMR (400 MHz, $CDCl_3$): δ = 9.33 (s, 2H, *H*-10), 9.14 (s, 2H, *H*-5), 3.55 – 3.17 (m, 8H, *H*-1',1''), 2.89 (s, 6H, *H*-1'''), 1.50 (t, ^3J = 7.7 Hz, 6H, *H*-2'), 1.35 (t, *J* = 7.7 Hz, 6H, *H*-2'') ppm.

^{13}C-NMR (101 MHz, $CDCl_3$): δ = 162.91 (q, *C*-1,4), 162.30 (q, *C*-9), 154.90 (q, *C*-6), 140.70 (q, *C*-7), 137.67 (q, *C*-2,3), 133.38 (q, *C*-8), 120.41 (t, *C*-10), 112.79 (t, *C*-5), 19.03 (s, *C*-1'), 18.74 (s, *C*-1''), 17.41 (p, *C*-2''), 16.49 (p, *C*-2'), 10.71 (p, *C*-1''') ppm.

HRMS (ESI, 70 eV): *m/z calcd for $C_{26}H_{31}N_3O_3Re$:* 620.19 *$[M+H]^+$; Found:* 620.19.

IR: $\tilde{\nu}$ = 2965 (m), 2929 (m), 2869 (m), 1487 (w), 1453 (s), 1411 (w), 1377 (w), 1312 (w), 1272 (w), 1261 (w), 1231 (w), 1175 (w), 1145 (m), 1113 (w), 1057 (m), 1023 (w), 1003 (w), 969 (w), 949 (w), 928 (s), 899 (vs), 885 (s), 812 (s), 763 (w), 747 (w), 728 (s), 646 (w), 495.19 (w),, 466 (w), 428 (w), 377 (s), 355 (w), 334 (w), 318 (w) cm^{-1}.

Raman: $\tilde{\nu}$ = 3050 (w), 2968 (m), 2931 (s), 2869 (m), 1562 (s), 1541 (s), 1491 (s), 1453 (w), 1392 (m), 1356 (w), 1313 (w), 1285 (s), 1233 (m), 1213 (m), 1149 (w), 1114 (w), 1062 (w), 1025 (w), 996 (w), 971 (w), 929 (m), 903 (m), 826 (w), 818 (w), 765 (w), 727 (w), 710 (w), 645 (m), 602 (w), 394 (w), 383 (w), 359 (m), 262 (w), 236 (w), 186 (w), 163 (m) cm^{-1}.

UV/Vis (CH_2Cl_2): λ_{max} (ε) = 233 (15450), 352 (38725), 511 (4705), 545 (3390) nm.

3. Oxygenation Experiments

3.1 Oxidation of Triphenylphosphine

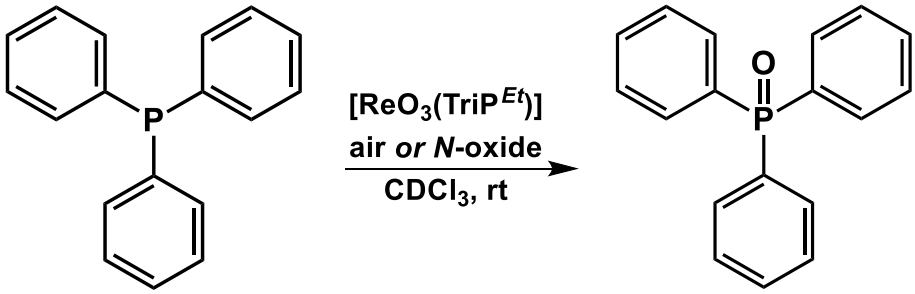

The catalysis experiment was executed following a similar approach based on FURUTA *et al*. Reaction was executed in a NMR-tube with $CDCl_3$ as solvent. The reaction was achieved with 4-phenylpyridine-*N*-oxide/O_2 at room temperature in the presence of 0.3 /2.5 mol % of [ReO_3(TriP^{Et})] (**3**) and conversion rate followed by $^{1}H/^{31}P$-NMR spectroscopy.

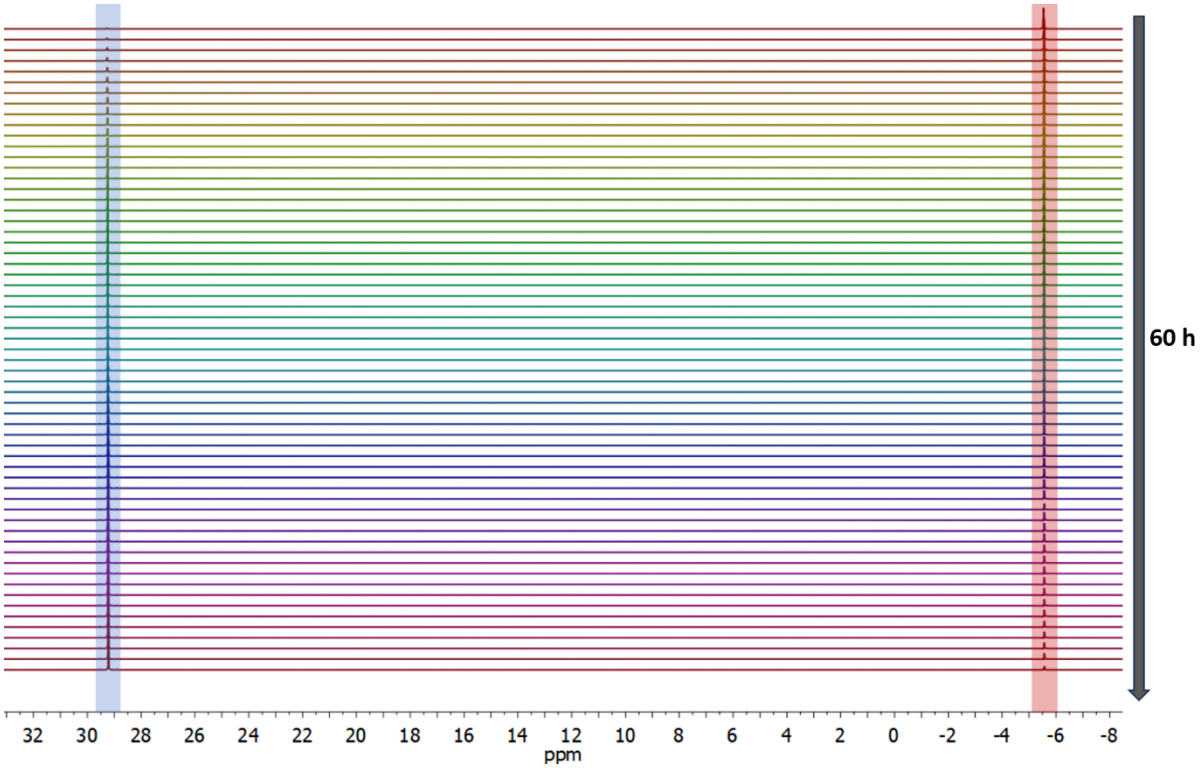

Figure S1. ^{31}P-NMR spectra of the catalytic conversion of PPh_3 with 4-phenylpyridine-*N*-oxide. Based on literature the signals at 29.27 ppm (blue) can be ascribed to $OPPh_3$ and -5.54 ppm (red) to PPh_3.[13, 14]

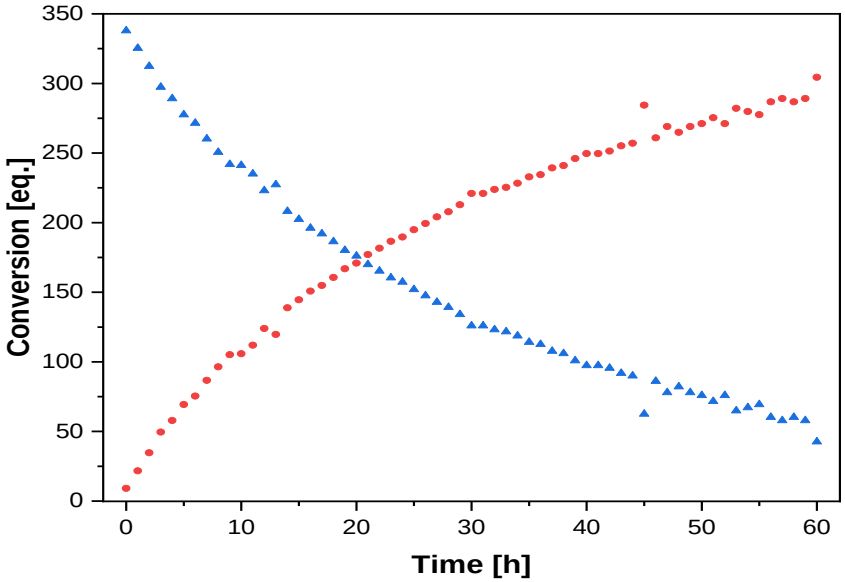

Figure S2. Equimolar catalytic conversion of PPh_3 (blue) to $OPPh_3$ (red) with 4-phenylpyridine-*N*-oxide over time with **3** as catalyst.

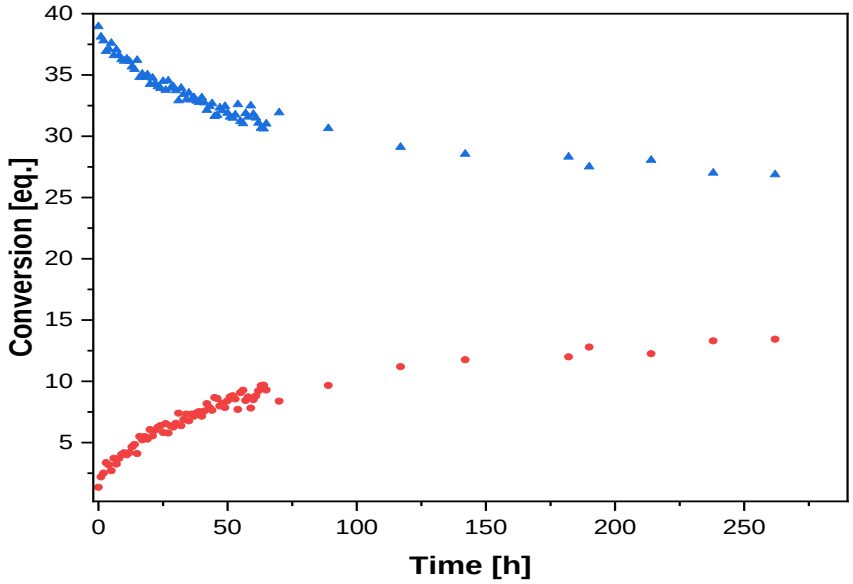

Figure S3. Equimolar catalytic conversion of PPh_3 (blue) to $OPPh_3$ (red) with O_2 over time with **3** as catalyst.

3.2 Oxygenation of Cyclooctene

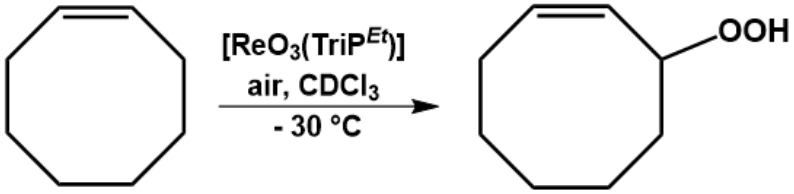

Reaction was executed in a NMR-tube with $CDCl_3$ as solvent. Under air conditions and at -30°C Cyclooctene in the presence of 5 mol % of [ReO_3(TriP^{Et})] (**3**) and 365 nm light irradiation. Conversion rate followed by ^{1}H-NMR spectroscopy. Followed after with mass spectrometry for verification of the resulting products.

Control experiments were executed under the identical conditions at ambient temperature and -30°C without catalyst **3** to verify that no other reactions falsify the catalytic results.

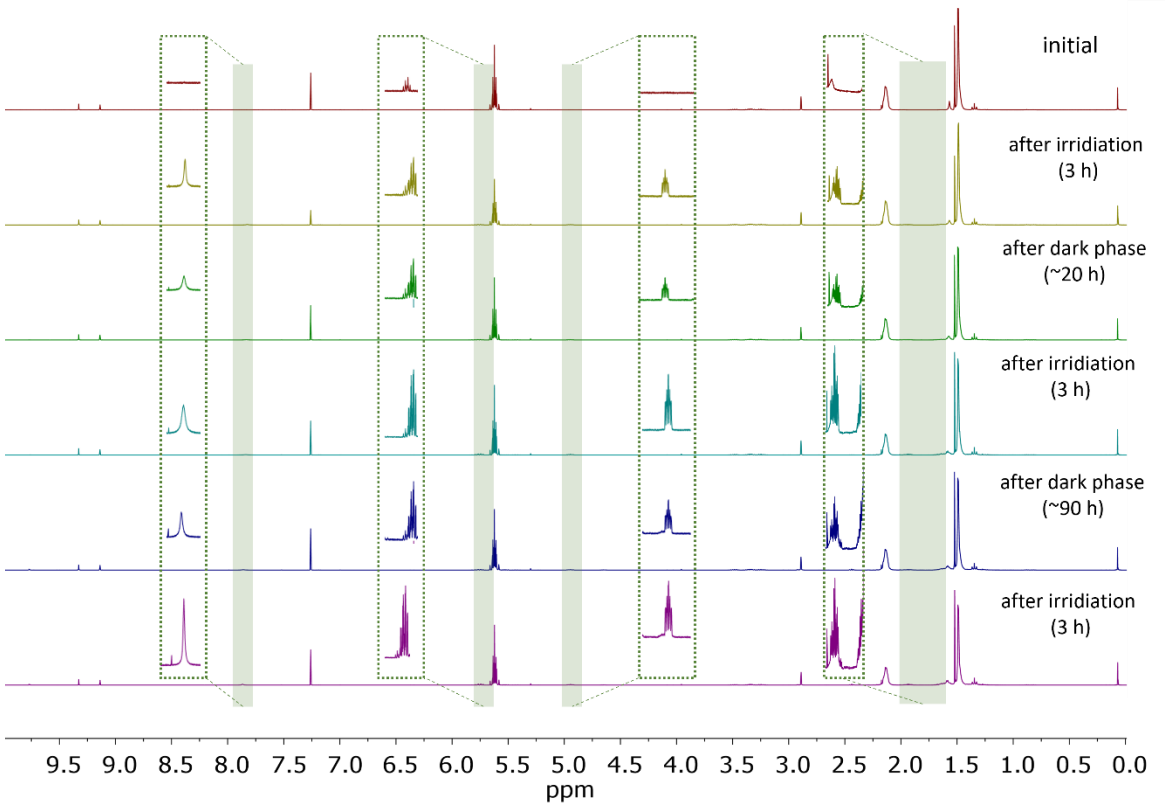

Figure S4. ^{1}H-NMR spectra of the catalytic conversion of cyclooctene to cyclooct-2-ene hydroperoxide with **3** as catalyst. Based on literature the arising signals (green) are ascribed to cyclooct-2-ene hydroperoxide.[15]

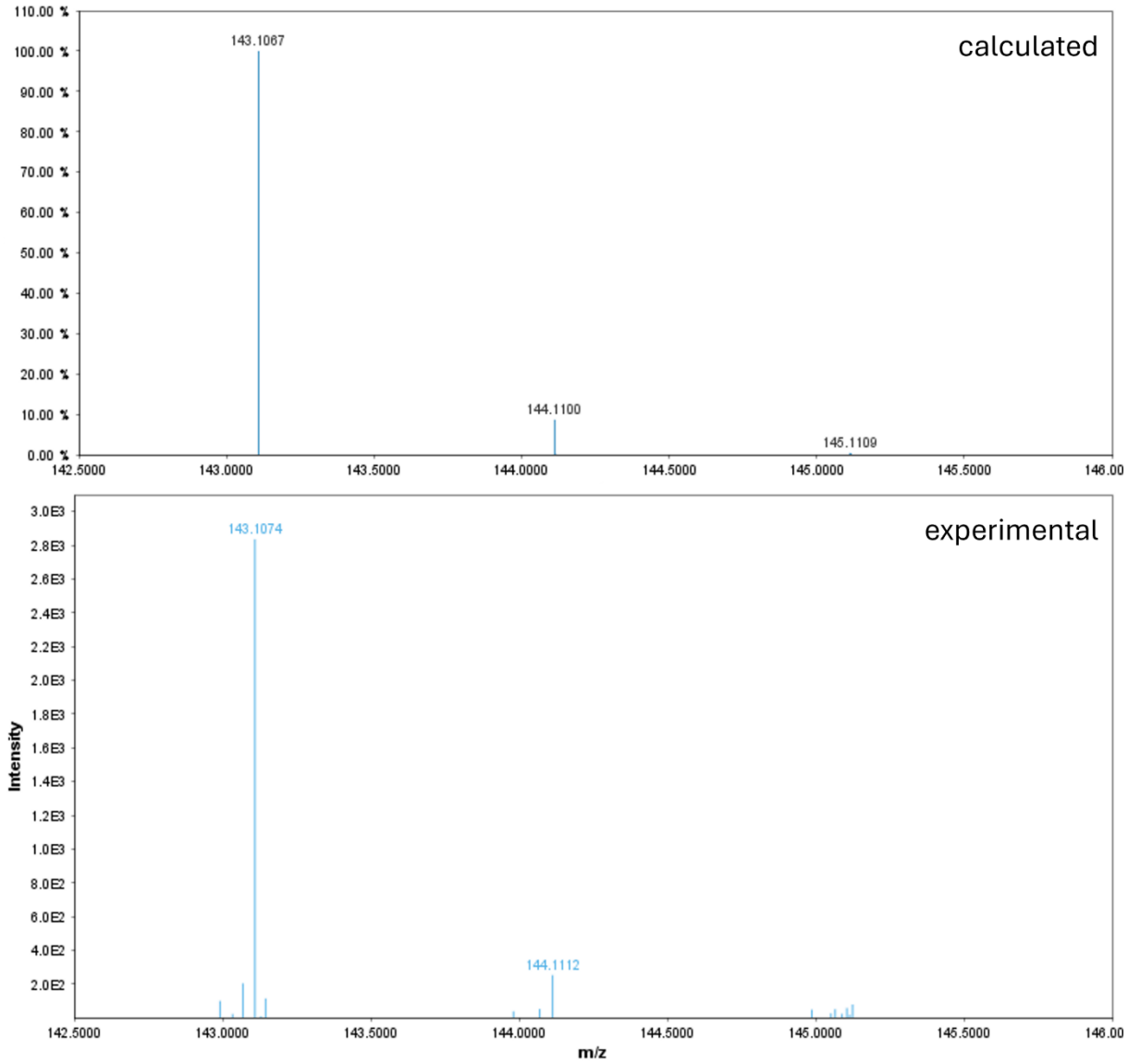

Figure S5. ESI mass spectra of cyclooct-2-ene hydroperoxides ($[M+H]^+$) after 3 h of irradiation.

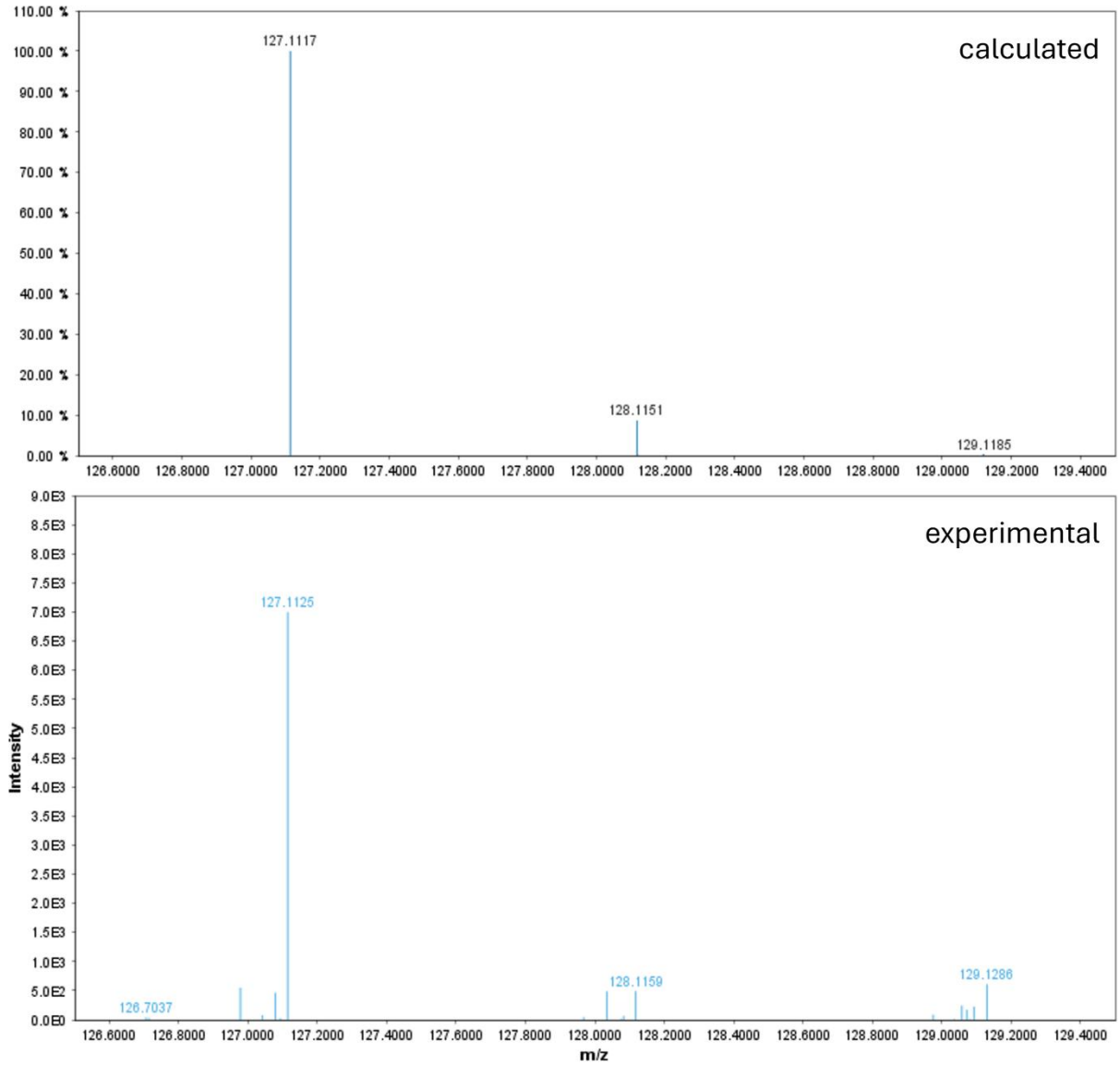

Figure S6. ESI mass spectra of 2-cyclooctene-1-ol ($[M+H]^+$) after 3 h of irradiation.

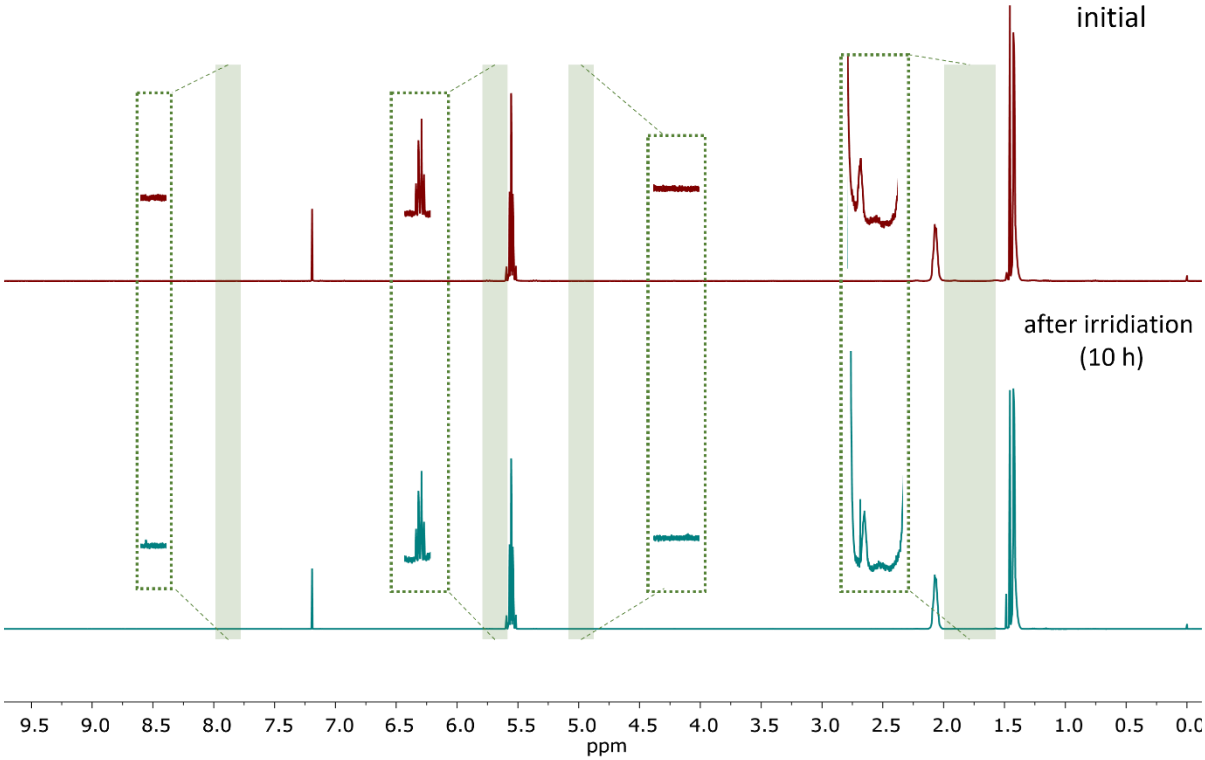

Figure S7. ^{1}H-NMR spectra of the control experiment. After 10 h irradiation no significant signals for cyclooct-2-enen hydroperoxides are arising therefore indicating that photooxygenation only occurs with the catalyst **3**.

4. NMR Spectroscopy

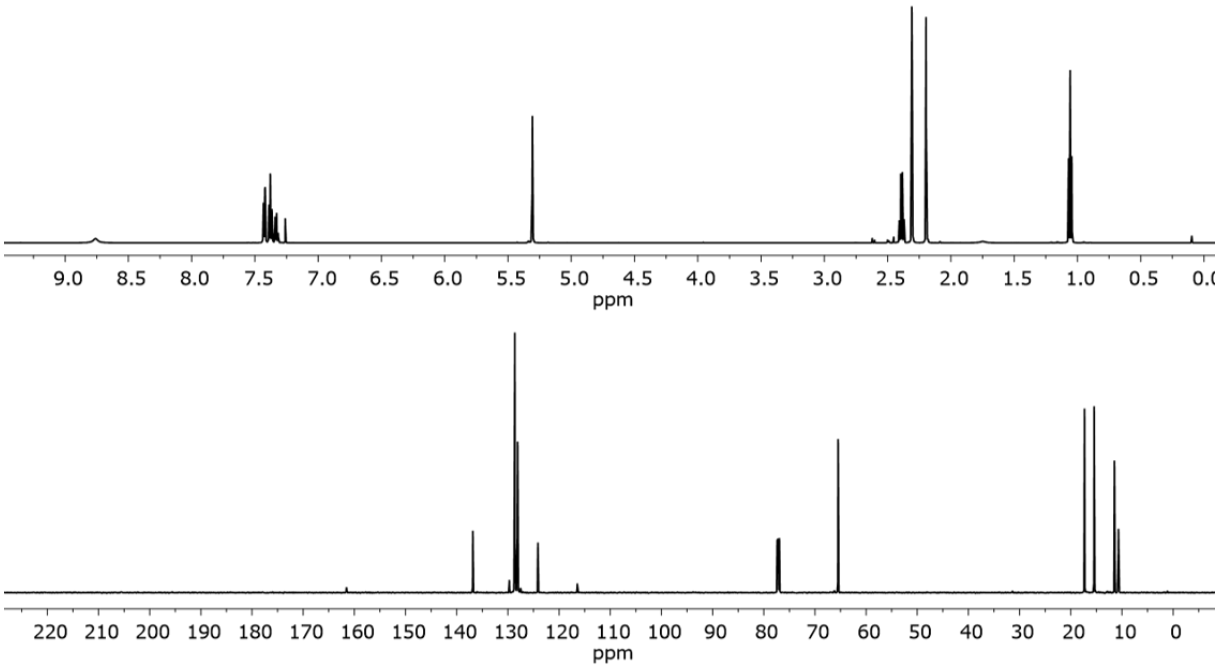

Figure S8. ^{1}H-NMR and ^{13}C-NMR spectra of compound **4**.

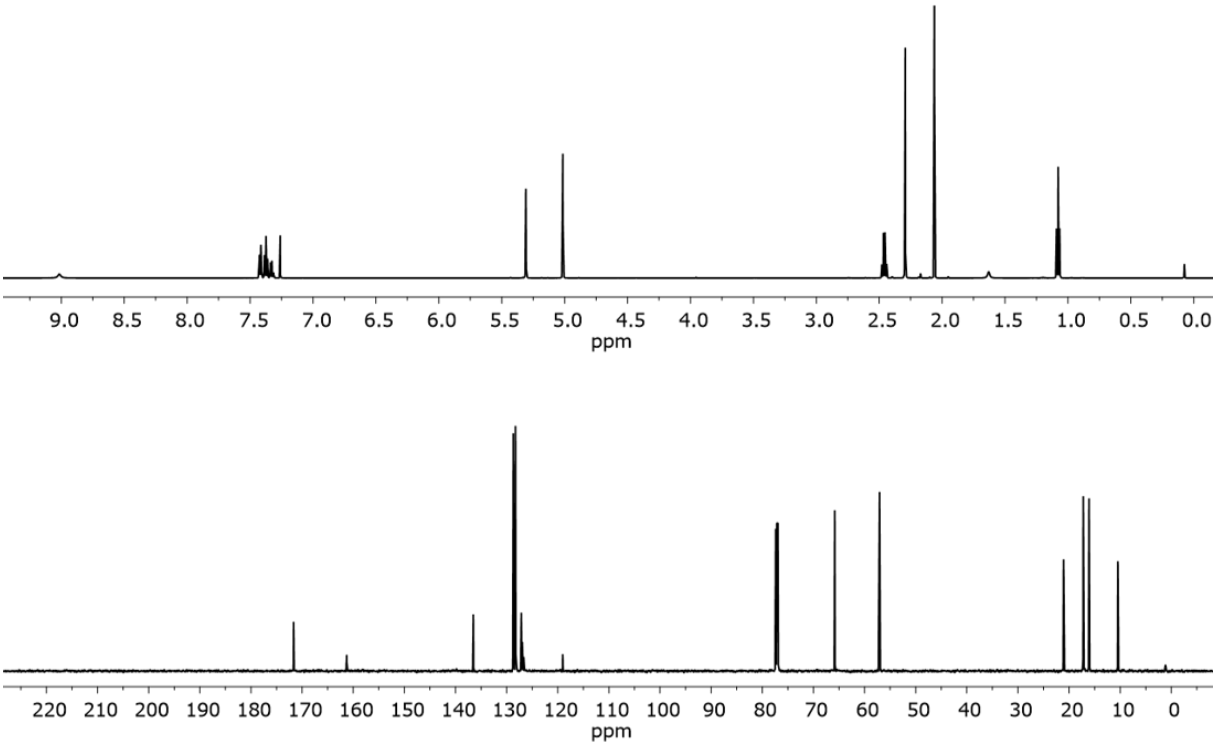

Figure S9. ^{1}H-NMR and ^{13}C-NMR spectra of compound **5**.

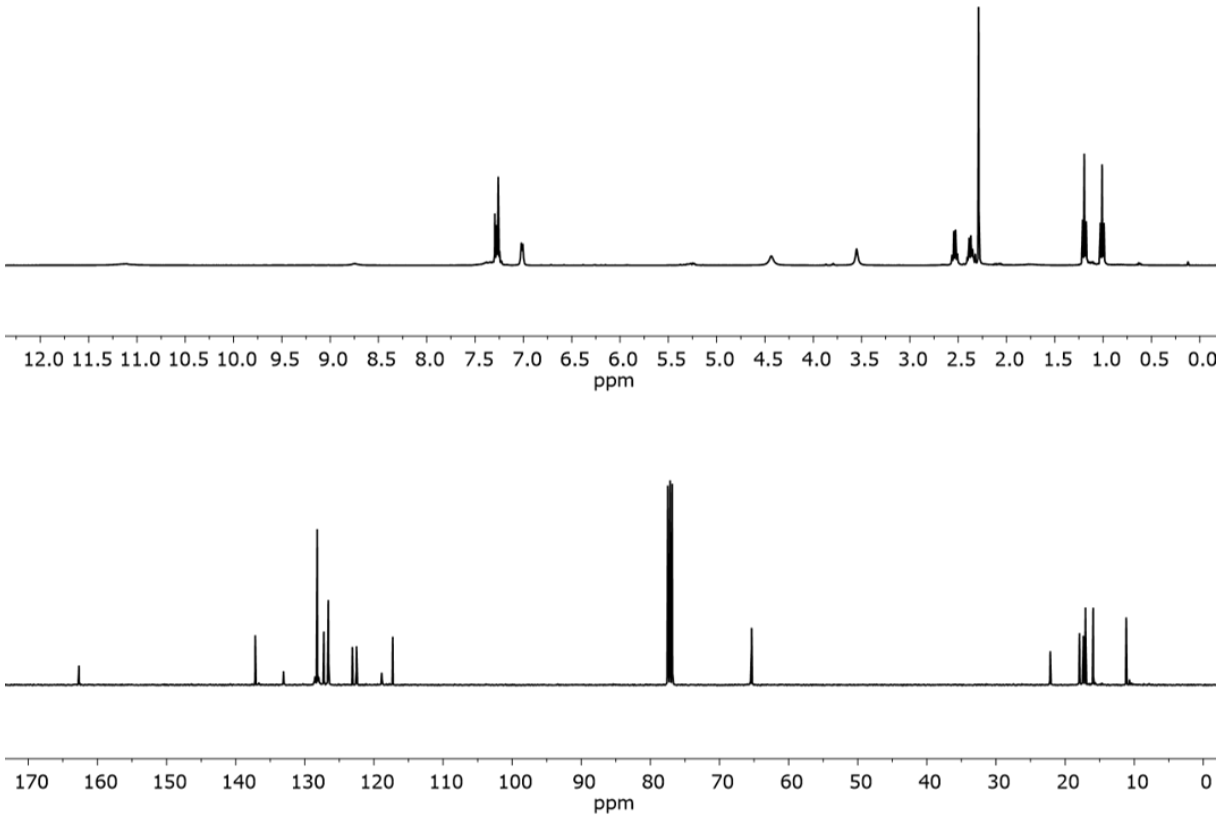

Figure S10. ^{1}H-NMR and ^{13}C-NMR spectra of compound **6**.

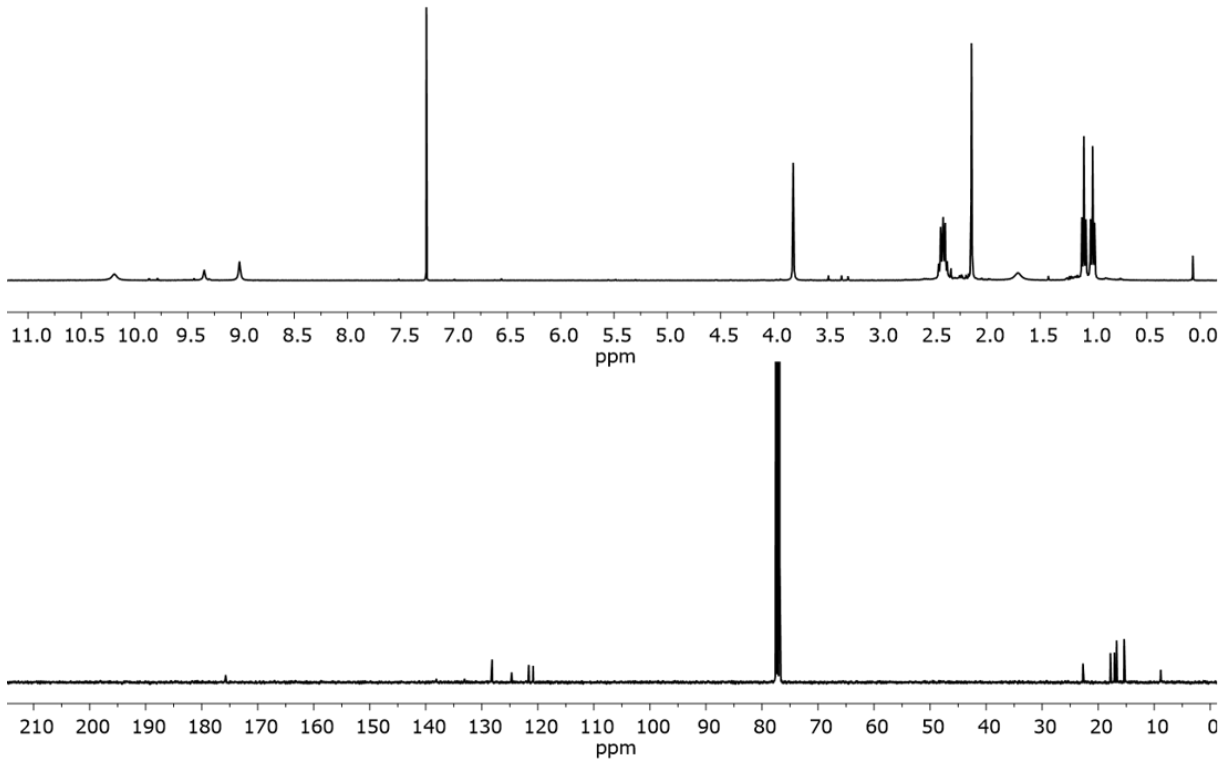

Figure S11. ^{1}H-NMR and ^{13}C-NMR spectra of compound **7**.

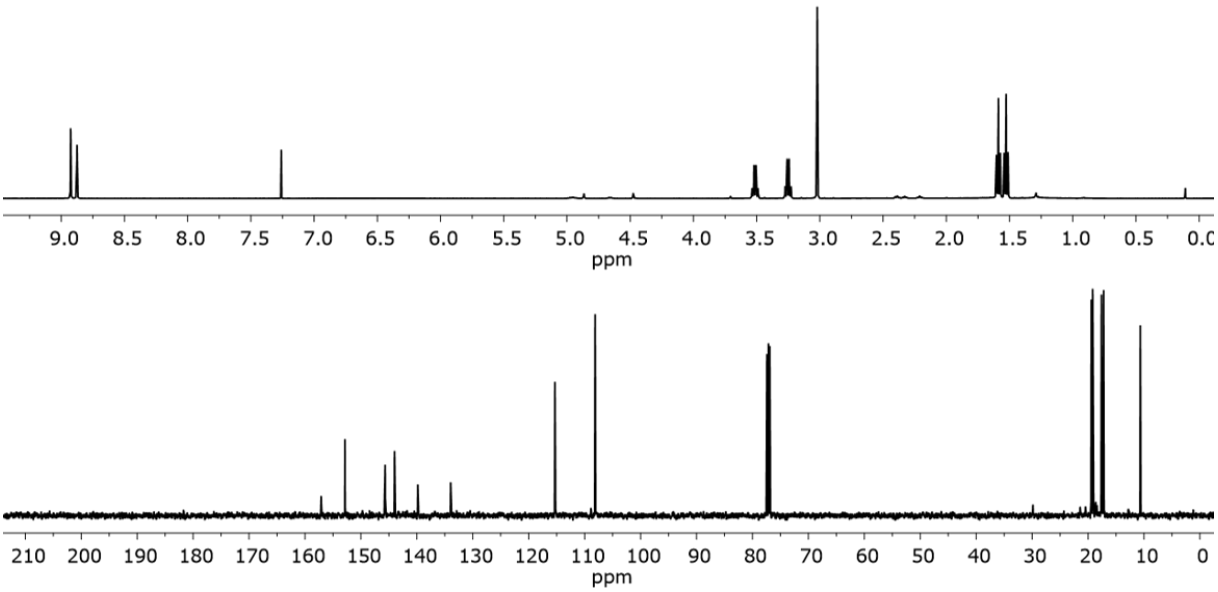

Figure S12. ^{1}H-NMR and ^{13}C-NMR spectra of TriP^{Et} **1**.

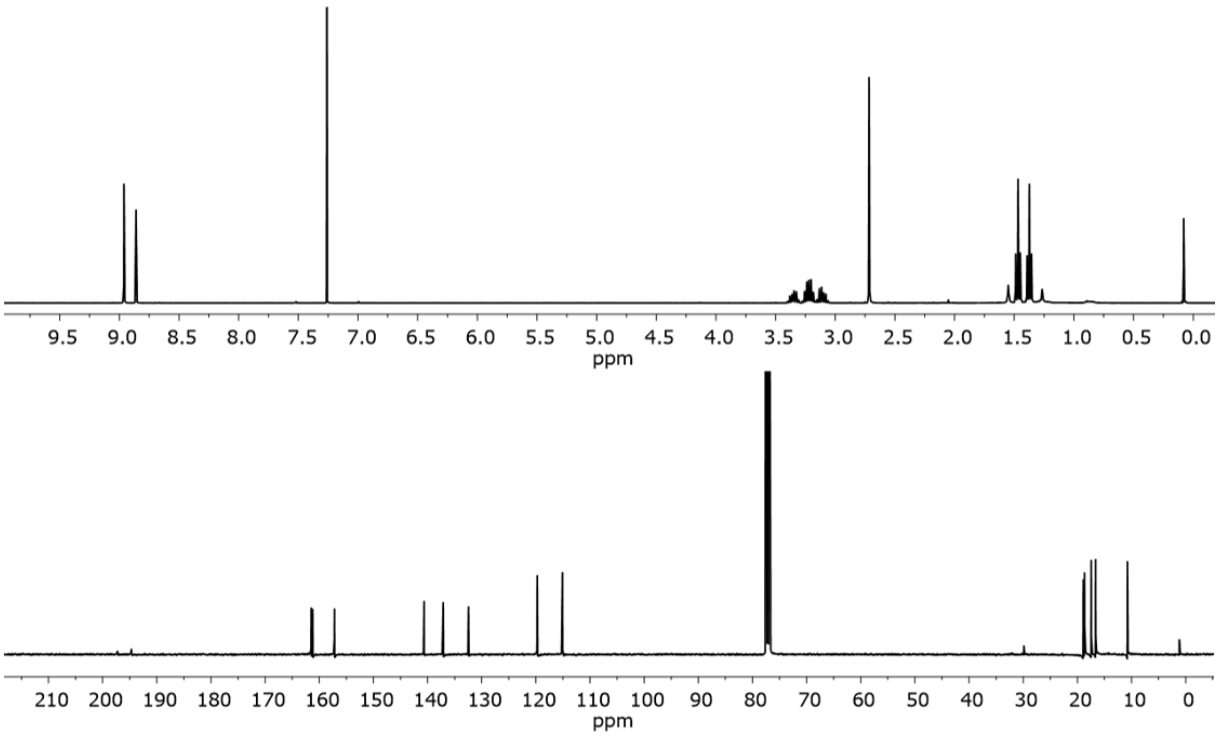

Figure S13. ^{1}H-NMR and ^{13}C-NMR spectra of [Re (TriP^{Et})(CO)$_3$] (**2**).

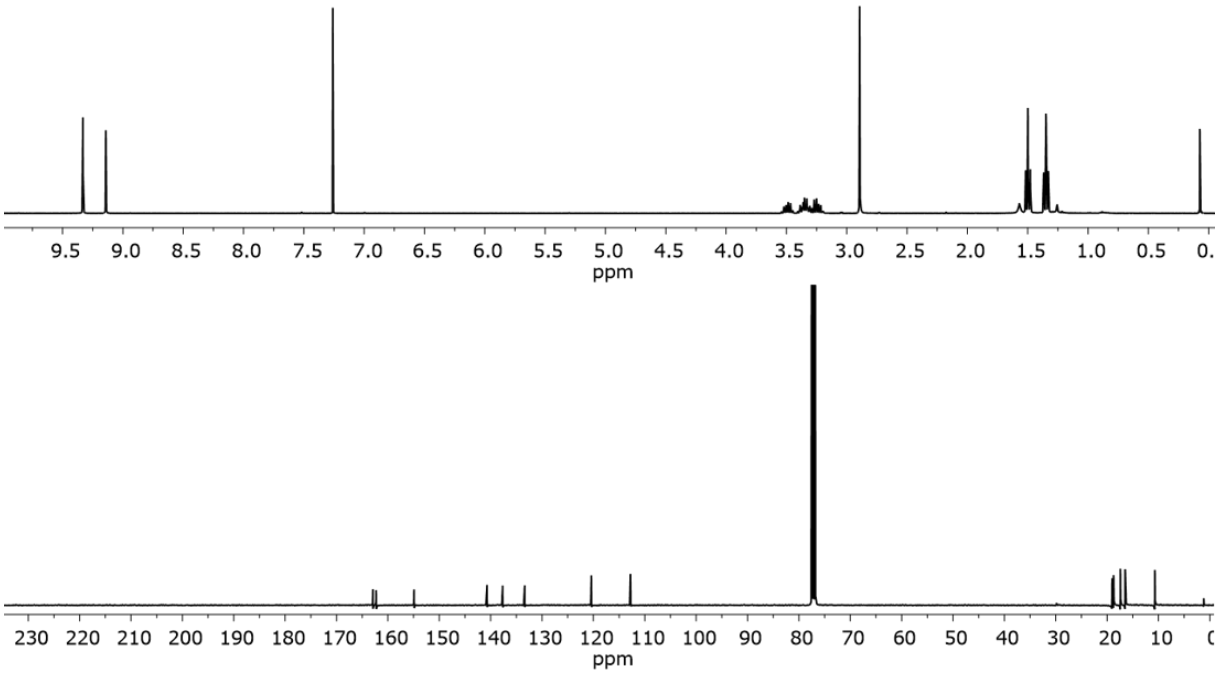

Figure S14. ^{1}H-NMR and ^{13}C-NMR spectra of [ReO_3(TriP^{Et})] (**3**).

5. UV/Vis Spectroscopy

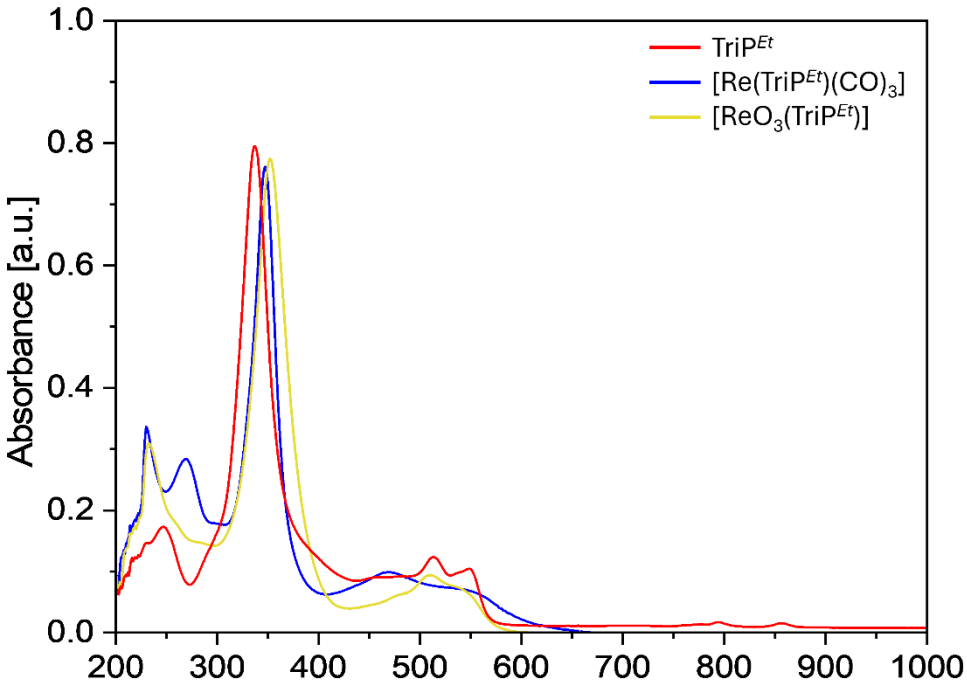

Figure S15. UV/Vis spectra of TriP^{Et} (**1**, red), [Re(TriP^{Et})(CO)$_3$] (**2**, blue) and [ReO$_3$(TriP^{Et})] (**3**, green) in CH_2Cl_2. All solutions were prepared at a concentration of 0.2 mmol·L^{-1}. The intensity of the spectrum of **1** was reduced by a factor of 0.5 to allow for better comparison with the other spectra.

Analogous to the triphyrin(2.1.1) system reported by YAMADA *et al.*,[16] the most intense absorption band of the TriP^{Et} ligand (**1**) is observed at 337 nm, comparable to the Soret band of porphyrins. The corresponding Q-band analogues are located at 514 and 548 nm.

6. Single Crystal X-Ray Structure Determination

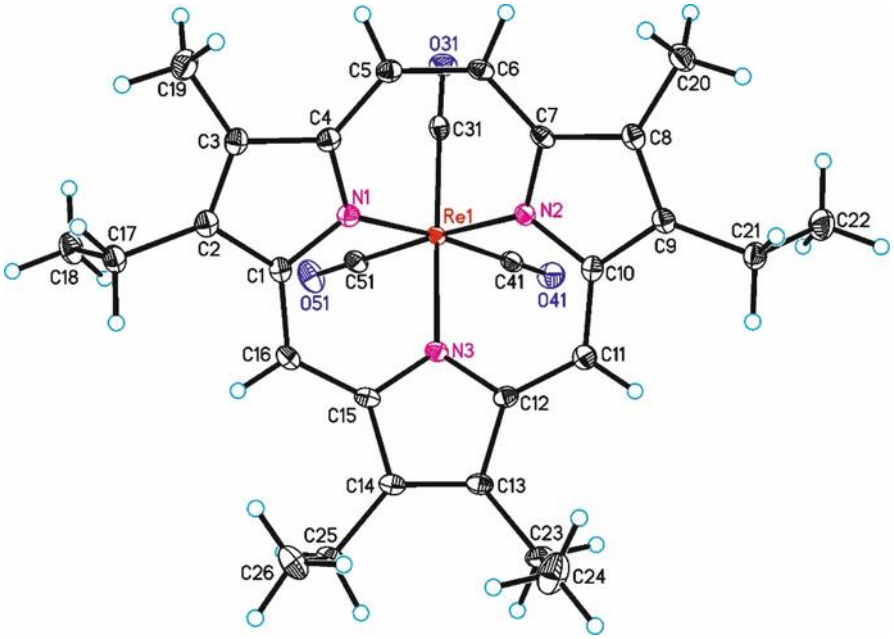

Figure S16. Molecular structure of [Re(TriP^{Et})(CO)$_3$] (**2**) with labeling and displacement ellipsoids drawn at the 50 % probability level.

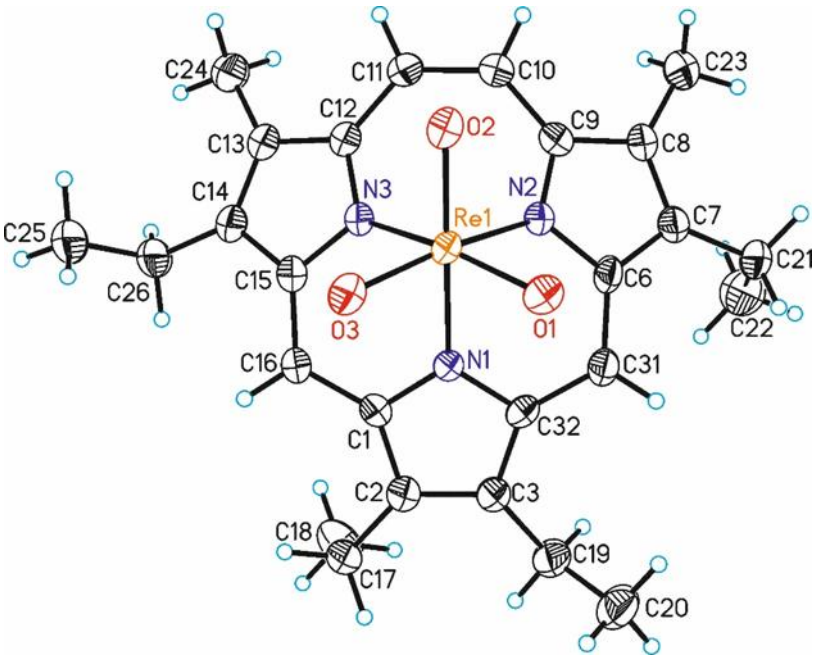

Figure S17. Molecular structure of [ReO$_3$(TriP^{Et})] (**3**) with labeling and displacement ellipsoids drawn at the 50 % probability level.

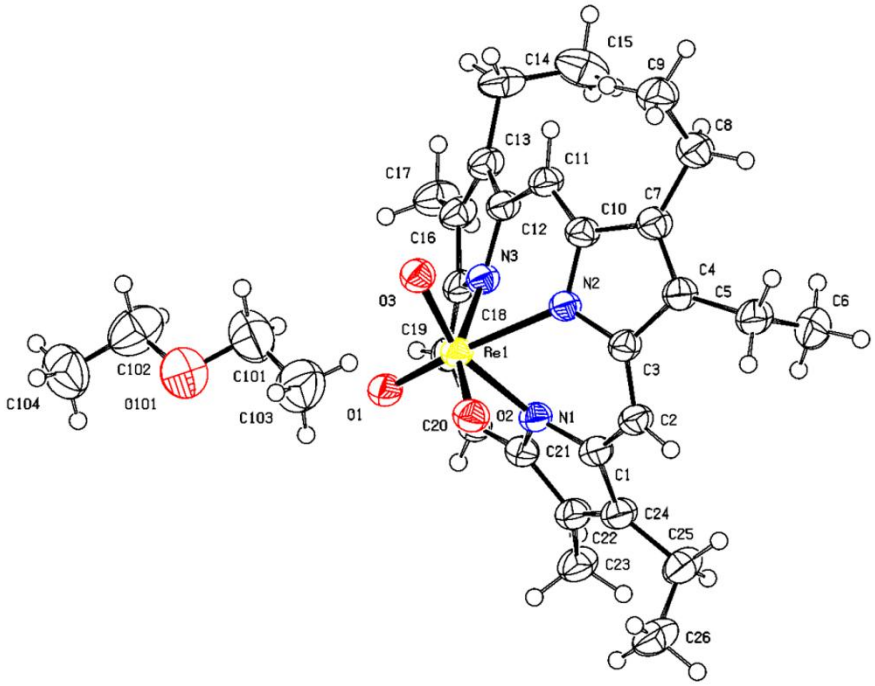

Figure S18. Molecular structure of [$ReO_3(TriP^{Et})$] with diethylether solvate **(3-Et_2O)** with labeling and displacement ellipsoids drawn at the 50 % probability level.

Table S1. Selected crystal data and structure refinement for [$Re(TriP^{Et})(CO)_3$] (**2**), [$ReO_3(TriP^{Et})$] (**3**) and [$ReO_3(TriP^{Et})$] with diethylether solvate (**3-Et_2O**).

Compound	**2**	**3**	**3-Et_2O**
Empirical formula	$C_{29}H_{30}N_3O_3Re$	$C_{26}H_{30}N_3O_3Re$	$C_{30}H_{40}N_3O_4Re$
Formula weight	654.76	618.73	692.85
Temperature/K	100.00(10)	100.00(10)	100.00(10)
Crystal system	triclinic	monoclinic	monoclinic
Space group	P-1	C2/c	$P2_1/n$
a/Å	9.19418(7)	21.2187(3)	14.67065(7)
b/Å	10.16670(6)	11.70587(14)	11.75682(6)
c/Å	13.81606(6)	24.6546(3)	17.06503(10)
α/°	92.0104(4)	90	90
β/°	96.2968(5)	108.1324(14)	101.0758(5)
γ/°	97.2320(5)	90	90
Volume/$Å^3$	1271.880(13)	5819.70(14)	2888.56(3)
Z	2	8	4
$\rho_{calc}g/cm^3$	1.710	1.412	1.593
μ/mm^{-1}	9.633	8.384	8.538
F(000)	648.0	2448.0	1392.0
Crystal size/mm^3	0.2 × 0.13 × 0.03	0.2 × 0.16 × 0.02	0.07 × 0.05 × 0.02
2Θ range for data collection/°	6.444 to 159.726	7.546 to 155.386	7.288 to 160.21
Reflections collected	31276	52207	41023

Compound	**2**	**3**	**3-Et_2O**
R_{int}	0.0230	0.0445	0.0216
Independent reflections	5386	6122	6125
Reflections with [I>=2σ (I)]	5383	5860	5931
Parameters	332	304	351
Goodness-of-fit on F^2	1.075	1.065	1.094
R_1 [I>=2σ (I)]	0.0183	0.0290	0.0283
wR_2 [all data]	0.0499	0.0728	wR_2 = 0.0759
Largest diff. peak/hole / e $Å^{-3}$	0.96/-1.03	0.63/-1.56	1.90/-0.53

7. Vibrational Spectroscopy

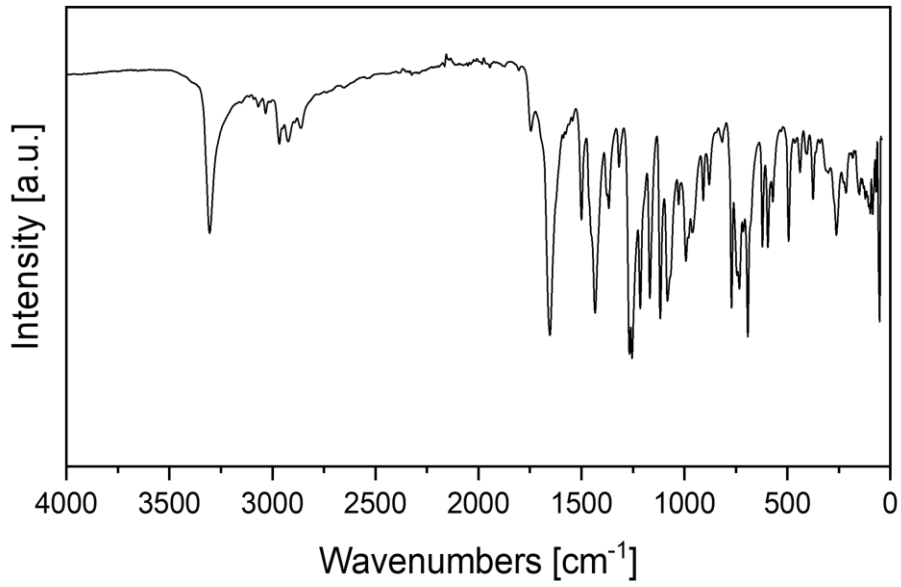

Figure S19. IR spectrum of compound **4**.

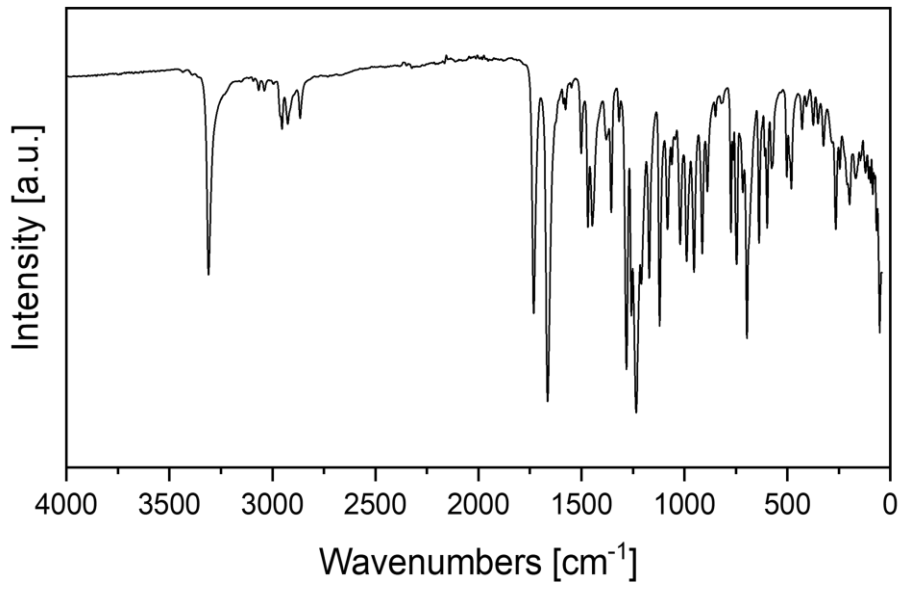

Figure S20. IR spectrum of compound **5**.

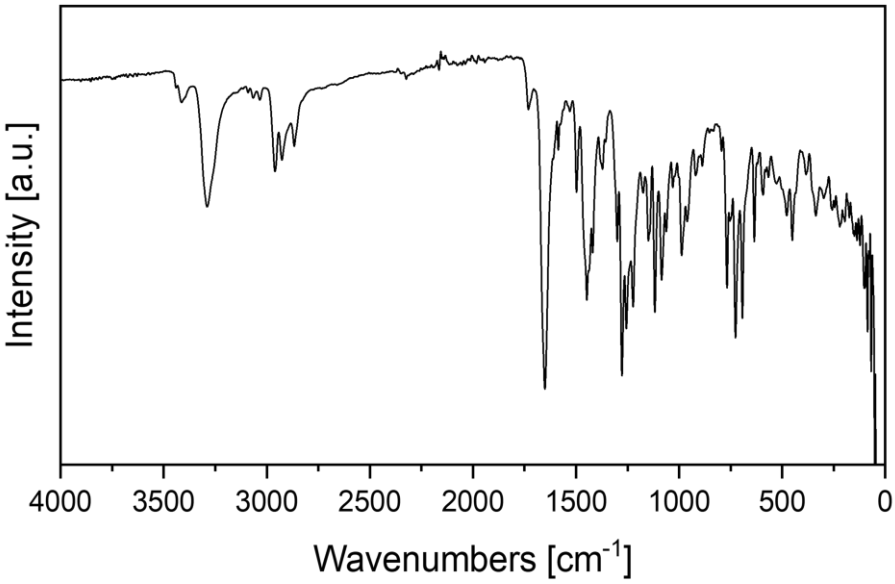

Figure S21. IR spectrum of compound **6**.

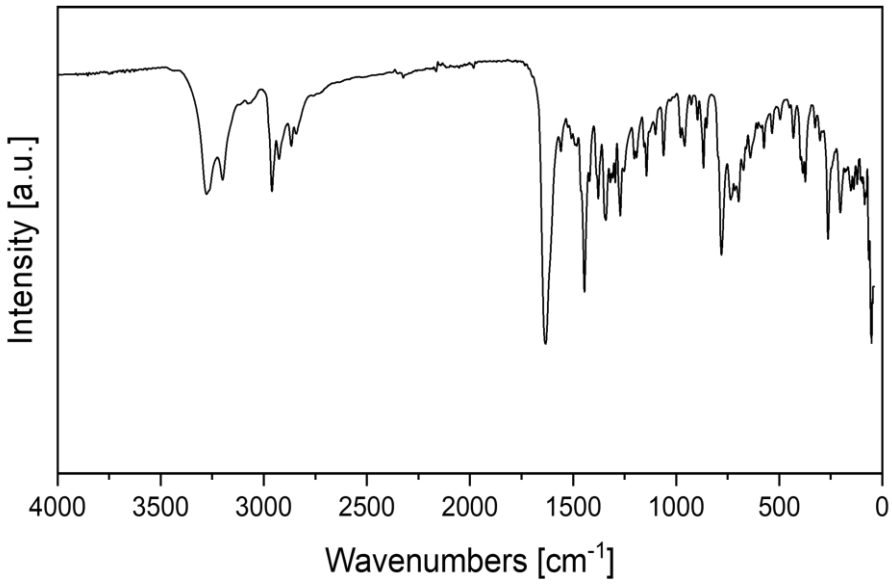

Figure S22. IR spectrum of compound **7**.

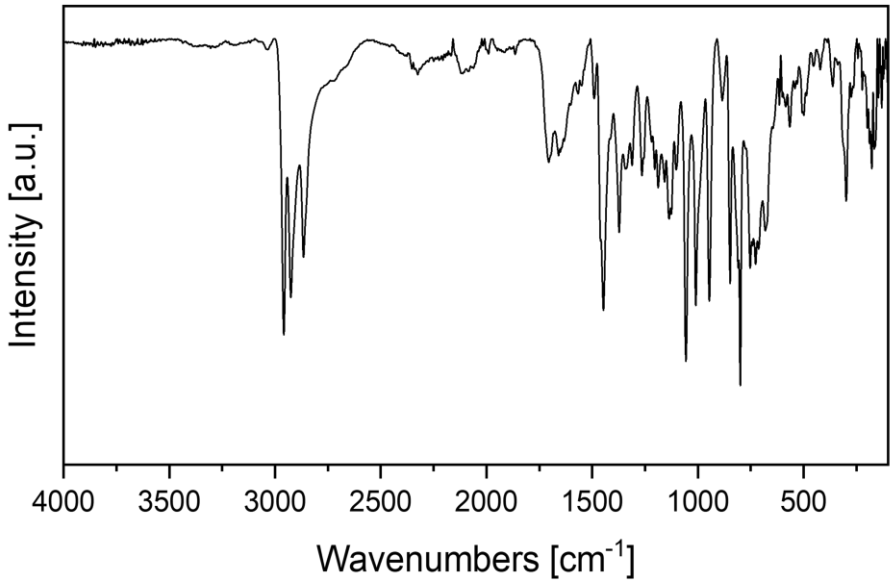

Figure S23. IR spectrum of TriP^{Et} (**1**).

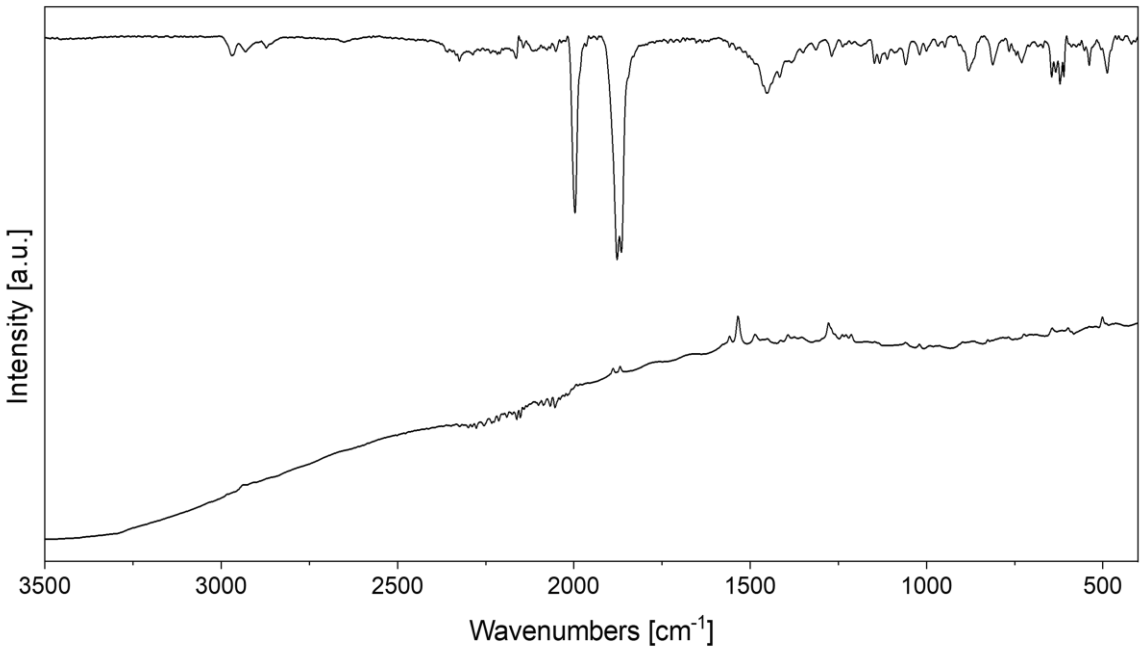

Figure S24. IR and Raman spectrum of [Re (TriP^{Et})(CO)$_3$] (**2**). Due to fluorescence of **2** the signals of the Raman spectrum are less resolved.

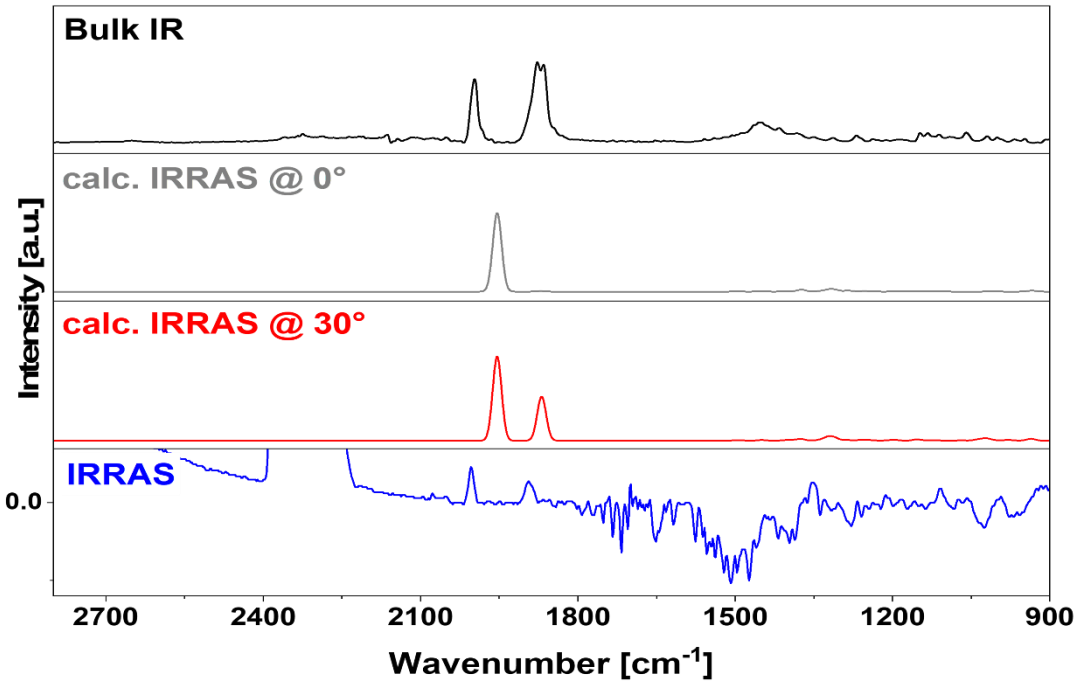

Figure S25. Overview spectra of calculated and measured vibrational spectra of [Re(TriP^{Et})(CO)$_3$] (**2**) both in bulk material and after adsorption on Au(111) surfaces**.**

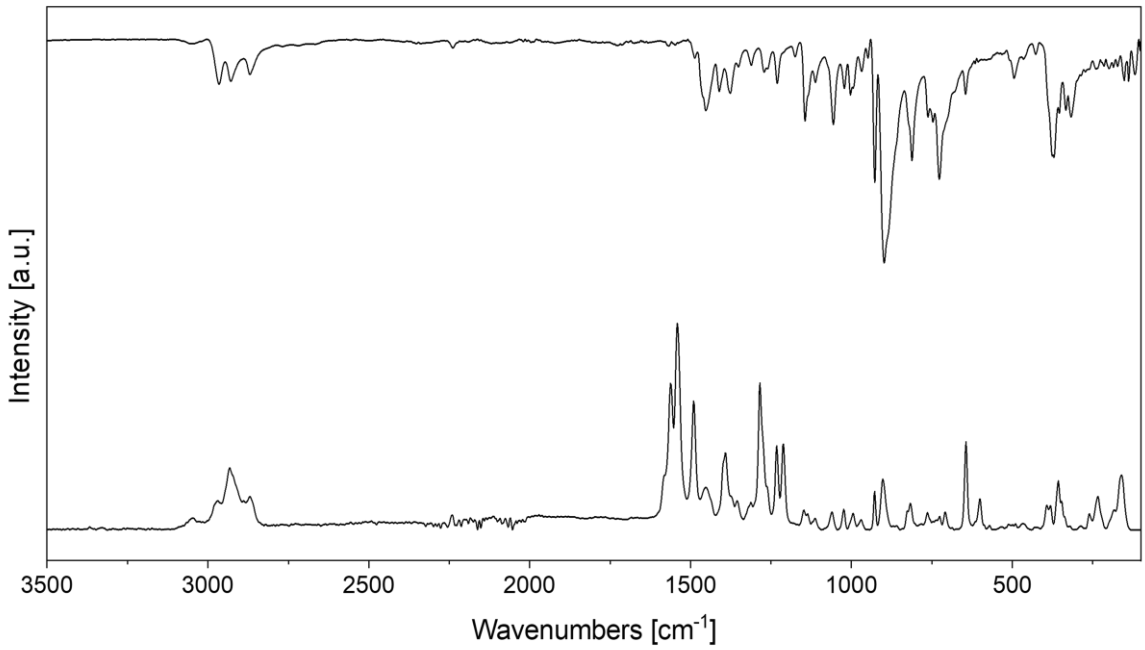

Figure S26. IR and Raman spectrum of [ReO$_3$(TriP^{Et})] (**3**).

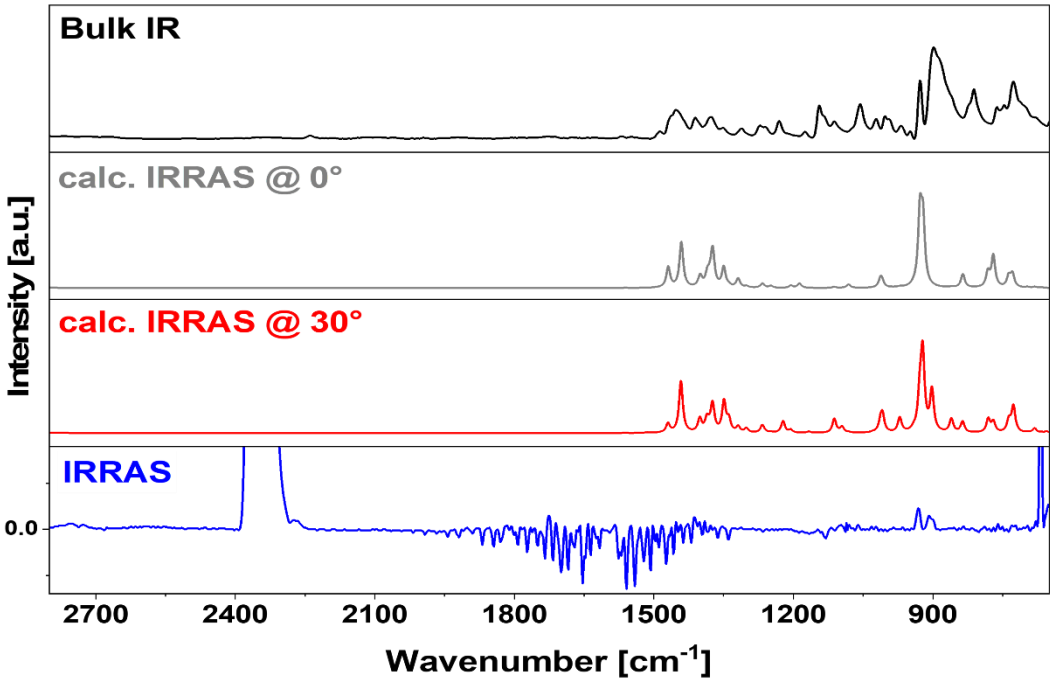

Figure S27. Overview spectra of calculated and measured vibrational spectra of [$ReO_3(TriP^{Et})$] (**3**) both in bulk material and after adsorption on Au(111) surfaces**.**

8. X-Ray Photoelectron Spectroscopy – XPS

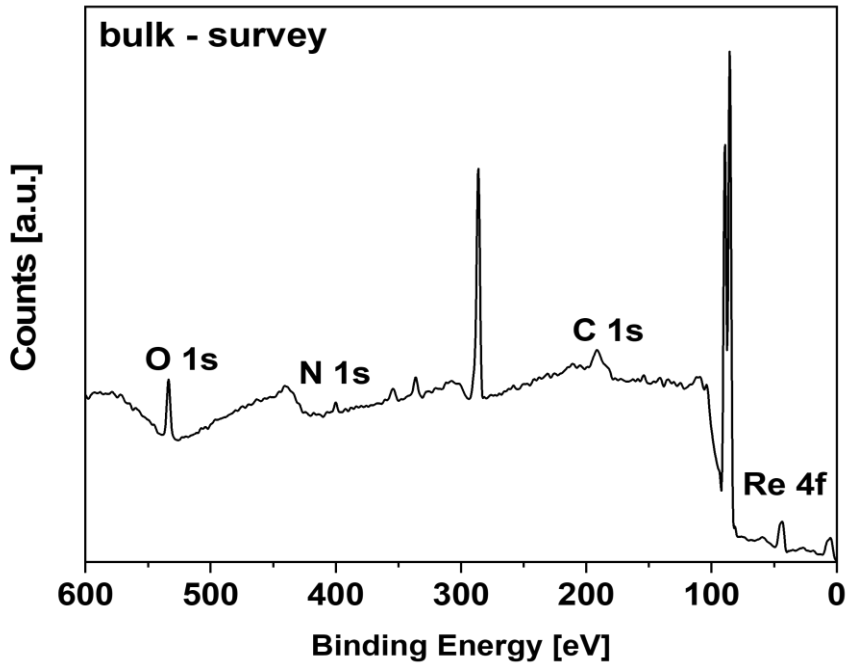

Figure S28. Survey spectra of [Re(TriP^{Et})(CO)$_3$] (**2**) in bulk form on Au(111).

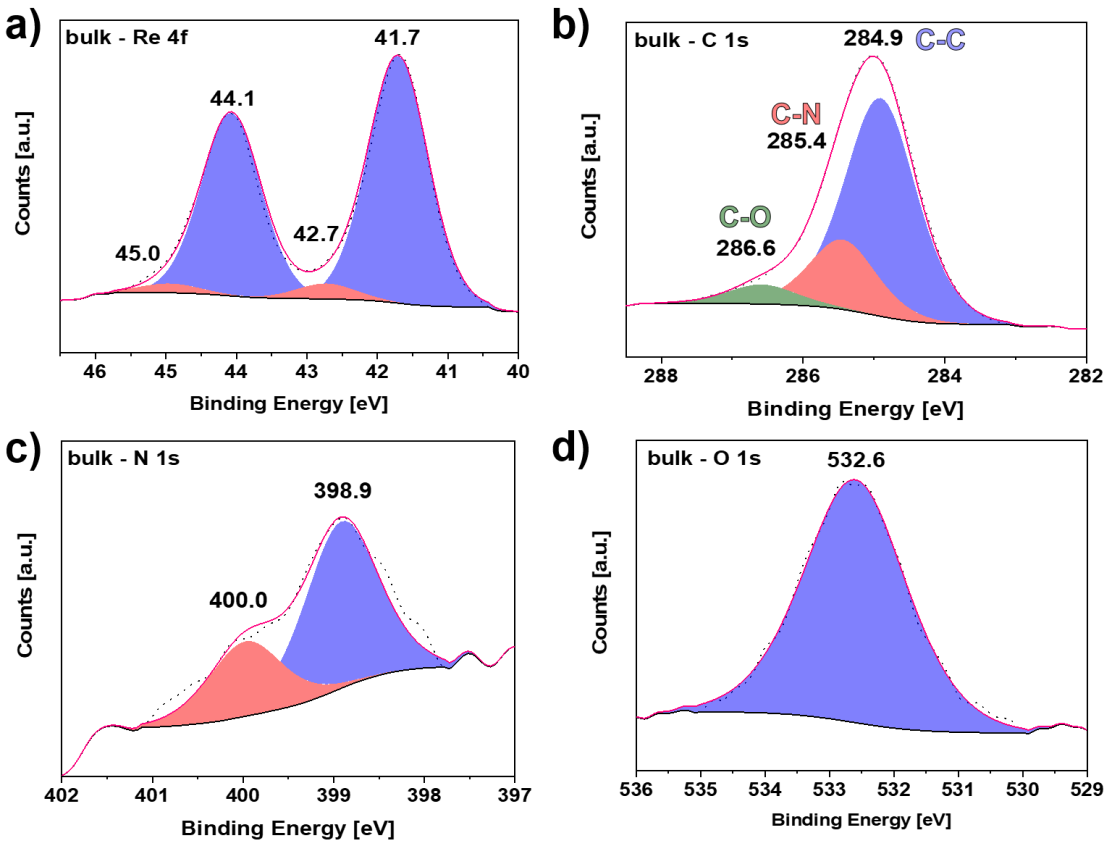

Figure S29. XP spectra of Re 4f (a), C 1s (b), N 1s (c), and O 1s (d) for [Re(TriP^{Et})(CO)$_3$] (**2**) as a thick layer on Au(111).

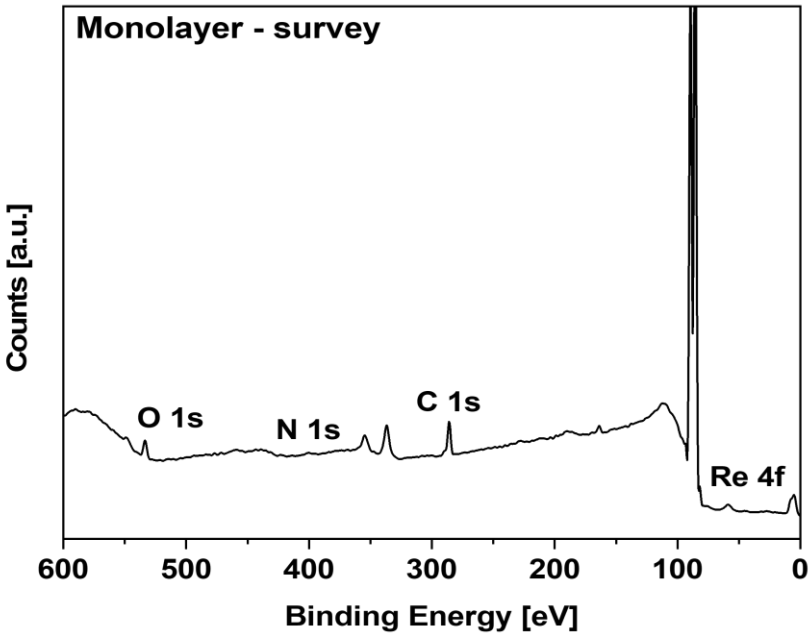

Figure S30. Survey spectra of [Re(TriP^{Et})(CO)$_3$] (**2**) as a monolayer on Au(111).

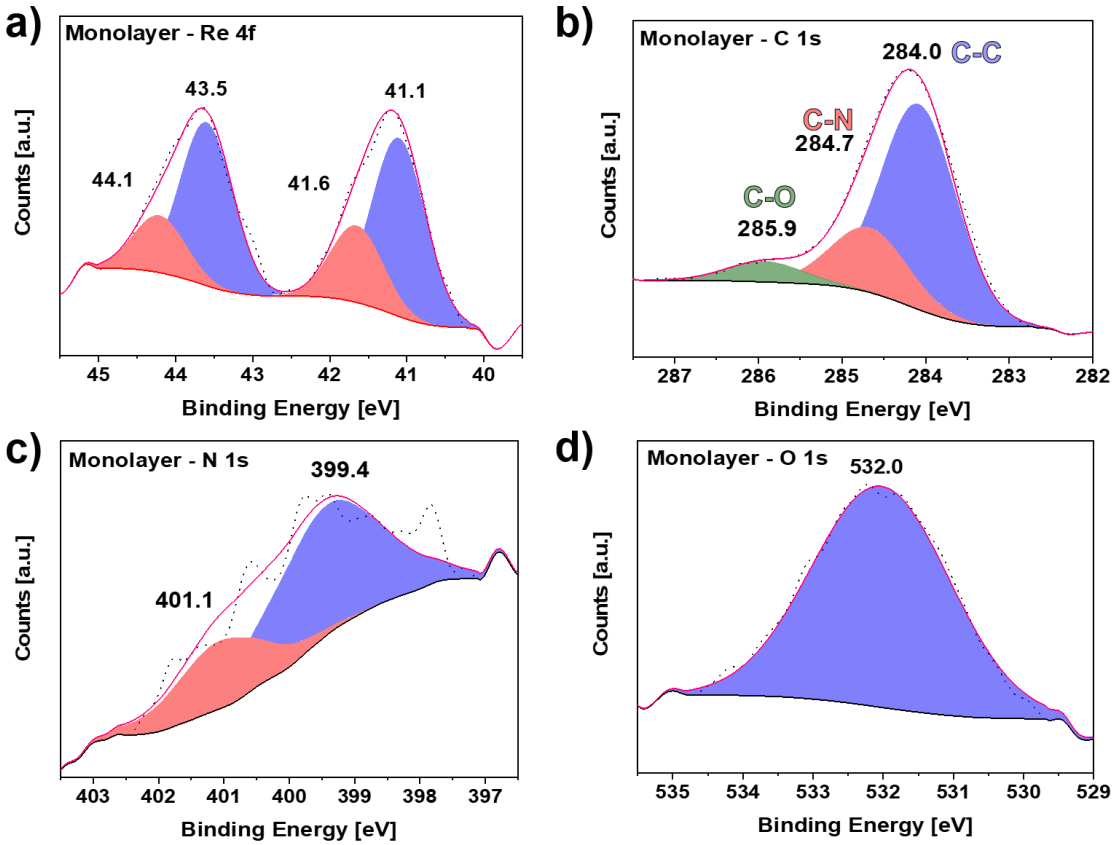

Figure S31. XP spectra of Re 4f (a), C 1s (b), N 1s (c), and O 1s (d) for a monolayer of [Re(TriP^{Et})(CO)$_3$] (**2**) on Au(111).

X-ray photoelectron spectroscopy (XPS) was employed to determine whether compound **2** remains intact and free of contamination after deposition onto Au(111) surfaces.

The survey spectra of **2** (Figure S27 and Figure S29) display the characteristic Au 4f peaks at 84.0 and 87.5 eV as well as Au 4d signals at 335.0 and 352.5 eV. Additionally, a well-defined C 1s peak is observed at 284.5 eV. The intensity ratio between the Au $4d_{5/2}$ and C 1s signals is consistent with the formation of a monolayer on Au(111) based on literature.[17–21]

The XP spectra are shown for a thick layer (corresponding to bulk) in Figure S28 and for a monolayer in Figure S30. In the bulk XP spectra (Figure S28 a), two sets of Re 4f signals are observed at 44.1/41.7 eV (blue) and 45.0/42.7 eV (red), each showing the expected spin–orbit splitting of ~2.4 eV and an intensity ratio of 4:3 corresponding to the $4f_{5/2}$ and $4f_{7/2}$ components. The relative ratio between the two species is approximately 94:6. The lower binding-energy component at 41.7 eV is consistent with Re(I) similar to reported literature values.[22–24] While the other species can be assigned to a higher oxidation state, which may originated from partial oxidation or decomposition, potentially due to interaction with trace amounts of water on the substrate surface or by intermolecular interactions.[23]

The C 1s spectrum (Figure S28 b) support this thesis, since the measured ratio between C-O, C-N and C-C is 6:22:73 and diverts from the expected ratio of 10:21:69, indicating the loss of CO species/ligands. The N 1s spectrum exhibits two peaks at 398.9 and 400.0 eV in a 2:1 ratio (Figure S28 c) respresenting the two distinct nitrogen of the triphyrin backbone, similarly to compound **3** and free-base porphyrins.[25–27] Finally, the O 1s region contains a broad peak at 532.1 eV, indicating the present of oxygen in form of carbonyl ligands (Figure 28 d).

The monolayer spectra (Figure S30) closely resemble the bulk data. However, a notable difference is that the amount of the species with higher binding energy is significantly higher than in the thick layer spectrum. This behavior is attributed to the greater exposure of the surface-bound species to X-ray irradiation whereas the Re complexes in the bulk material are partially shielded by outer layers. Additionally, in the monolayer the component at 44.1/41.6 eV (red), which was assigned to a higher oxidation state in the thick layer, shifts toward lower binding energy and is closer to that of the intact complex **2** at 43.5/41.1 eV (blue). In our previous study, it is shown

that a Mn(I) tricarbonyl triphyrin complex can lose carbonyl ligands on surface, while still remainining intact within the triphyrin framework.[28] Since Re(I) tricarbonyl complexes are known for dissociation of carbonyl ligands due to irradiation,[29] it is possible that, in monolayers, **2** is only partially losing CO ligands under the measurement conditions instead of undegoing oxidation.

We therefore postulate that interactions with the Au(111) substrate stabilize the surface-bound complex, resulting in the possible losses of CO ligand(s) but the rhenium metal center still remains as Re(I).

This interpretation is supported by the relative C 1s intensities observed for the monolayer. The experimental ratio of C–O, C–N, and C–C contributions of 7:22:71 diverts from the theoretical values, indicating the loss of CO ligands.

9. Near Edge X-Ray Absorption Fine Structure – NEXAFS

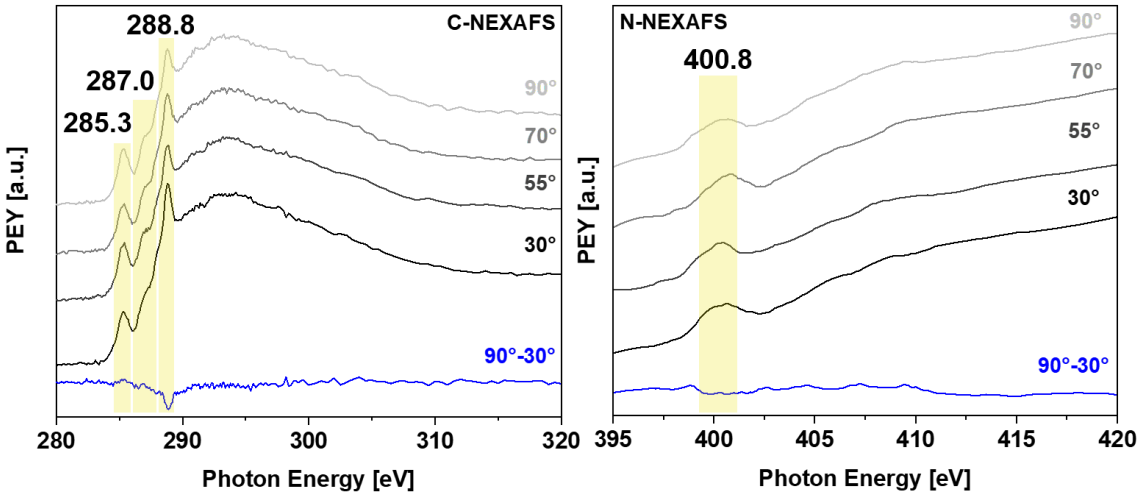

Figure S32. Normalized NEXAFS spectra of [Re(TriP^{Et})(CO)$_3$] (**2**) as a monolayer on Au(111) measured at incident angles of 30°, 55°, 70° and 90°.

Near-edge X-ray absorption fine structure (NEXAFS) spectroscopy was employed to further analyze the adsorption orientation of compound **2**. Carbon and nitrogen K-edges were recorded for a monolayer of [Re(TriP^{Et})(CO)$_3$] (***2***) on Au(111) at varying angles of incidence (Figure S31).

In the C K-edge spectrum, three π* resonances can observed. Based on literature data and structurally related systems, the signals at 285.3 eV and 288.8 eV are assigned to C 1s → π* transitions of the pyrrole units, while the resonance at 287.0 eV is attributed to the carbonyl ligands.[19,20,30,31] The first two transitions exhibit only weak angular dependence, with relatively minor changes in intensity between 30° and 90°. Noteably, the intensity difference between the angles from the C 1s → π* transition at 288.8 eV is clearly obeservable but non-vanishing. The carbonyl-related feature is comparatively weak and only barely distinguishable in the spectra.

The nitrogen K-edge spectrum displays a single π* resonance at 400.8 eV, corresponding to the N 1s → π* transition of the pyrrole nitrogen atoms.[19,31,32] Similar to the carbon K-edge, this transition shows only a slight decrease in intensity with increasing angle of incidence. Notably, a non-vanishing intensity remains at 90°, indicating that the pyrrole rings are not perfectly parallel to the surface but adopt a tilted orientation.

Overall, the observed intensity changes with varying angles of incidence indicate the presence of a preferential adsorption orientation on the surface. However, the non-vanishing π* intensities at 90° implicate that the complex is not adsorbed in a purely

horizontal geometry but instead adopts a tilted orientation relative to the substrate surface.

10. Computational Details

10.1 Coordinates of DFT calculated structures

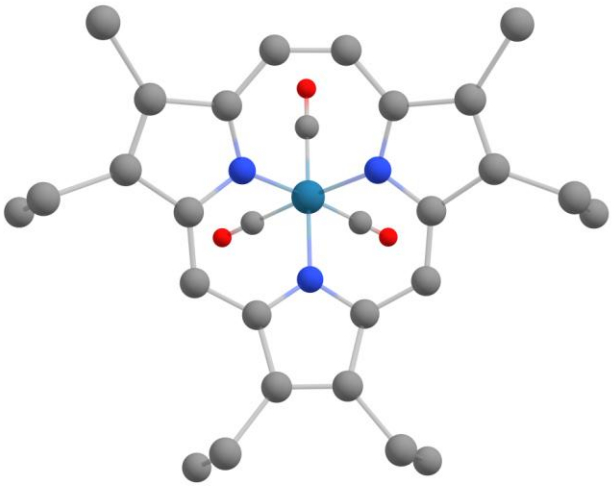

Figure S33. DFT calculated structure of [Re(TriP^{Et})(CO)$_3$] (**2**).

Table S2. Atomic coordinates of the DFT calculated structure of [Re(TriP^{Et})(CO)$_3$] (**2**).

	x	y	z		x	y	z
C	3.789	-0.933	1.932	**H**	-3.319	-0.297	-2.585
C	3.497	-0.752	3.268	**C**	-2.866	-0.972	5.494
C	2.167	-0.136	3.327	**H**	-2.251	-1.779	5.927
N	1.746	0.123	2.071	**H**	-2.803	-0.114	6.184
C	2.643	-0.415	1.185	**H**	-3.910	-1.316	5.489
C	2.336	-0.655	-0.166	**C**	4.304	-1.158	4.460
C	1.031	-0.572	-0.695	**H**	5.272	-1.587	4.164
C	-1.152	-0.522	-0.382	**H**	4.511	-0.297	5.117
C	-0.924	-1.350	-1.571	**H**	3.778	-1.910	5.072
C	0.444	-1.380	-1.767	**C**	5.008	-1.539	1.306
C	-2.258	-0.547	0.494	**C**	5.920	-0.496	0.640
C	-2.157	-0.305	1.875	**H**	5.578	-2.096	2.067
N	-1.019	0.178	2.468	**H**	4.699	-2.287	0.555
C	-1.083	-0.061	3.795	**H**	5.378	0.070	-0.134
C	-2.406	-0.604	4.120	**H**	6.287	0.232	1.380
C	-3.072	-0.761	2.922	**C**	-4.456	-1.285	2.680
C	1.386	0.011	4.503	**C**	-5.464	-0.173	2.354
C	0.004	0.044	4.702	**H**	-4.435	-2.015	1.852
H	1.965	-0.066	5.428	**H**	-4.798	-1.846	3.564
H	-0.294	-0.009	5.753	**H**	-5.536	0.546	3.185
C	1.234	-2.105	-2.815	**H**	-6.468	-0.588	2.169
C	1.876	-1.157	-3.841	**Re**	0.274	1.591	1.456
H	2.025	-2.704	-2.330	**C**	0.521	2.799	2.962
H	0.585	-2.827	-3.335	**C**	-1.196	2.680	0.806
H	2.545	-0.433	-3.349	**O**	-2.100	3.282	0.402
H	2.467	-1.719	-4.583	**O**	0.672	3.488	3.882
H	1.108	-0.580	-4.378	**N**	0.031	0.016	0.009

	x	y	z		x	y	z
C	-2.001	-2.033	-2.357	**C**	1.526	2.637	0.401
C	-2.830	-1.061	-3.211	**O**	2.286	3.218	-0.253
H	-1.553	-2.802	-3.007	**H**	-3.180	-1.008	0.134
H	-2.673	-2.574	-1.668	**H**	3.095	-1.161	-0.766
H	-2.191	-0.531	-3.934	**H**	6.792	-0.975	0.167
H	-3.614	-1.595	-3.772	**H**	-5.157	0.392	1.459

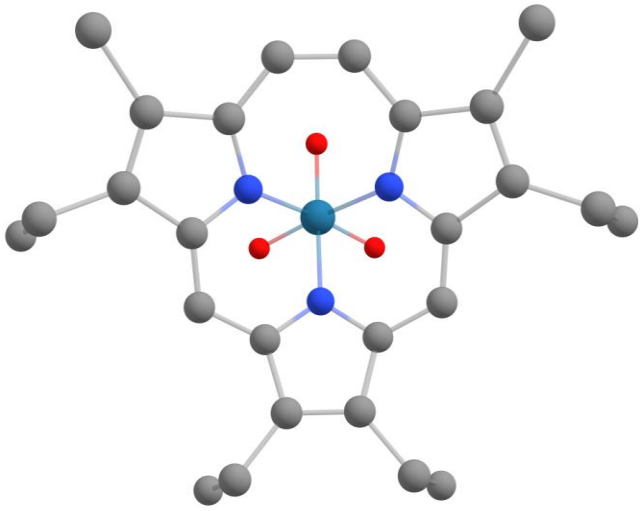

Figure S34. DFT calculated structure of [ReO_3(TriP^{Et})] (**3**).

Table S3. Atomic coordinates of the DFT calculated structure of [ReO_3(TriP^{Et})] (**3**).

	x	y	z		x	y	z
C	-2.215	-3.274	1.484	**H**	4.057	-4.188	5.108
C	-1.855	-3.105	2.805	**H**	4.643	-2.530	5.340
C	-0.497	-2.555	2.800	**H**	5.686	-3.737	4.560
N	-0.120	-2.321	1.519	**C**	-2.629	-3.463	4.033
C	-1.087	-2.807	0.682	**H**	-3.626	-3.851	3.782
C	-0.881	-2.997	-0.694	**H**	-2.769	-2.585	4.687
C	0.391	-2.884	-1.285	**H**	-2.112	-4.232	4.631
C	2.592	-2.817	-1.102	**C**	-3.501	-3.794	0.918
C	2.302	-3.553	-2.333	**C**	-4.402	-2.671	0.376
C	0.924	-3.593	-2.449	**H**	-4.044	-4.363	1.690
C	3.751	-2.862	-0.307	**H**	-3.283	-4.513	0.110
C	3.712	-2.671	1.084	**H**	-3.885	-2.090	-0.404
N	2.602	-2.219	1.744	**H**	-4.675	-1.969	1.179
C	2.752	-2.472	3.069	**C**	6.057	-3.656	1.738
C	4.099	-2.997	3.304	**C**	7.065	-2.538	1.432
C	4.690	-3.136	2.066	**H**	5.993	-4.338	0.872
C	0.341	-2.461	3.932	**H**	6.429	-4.268	2.574
C	1.733	-2.429	4.045	**H**	7.180	-1.867	2.298
H	-0.186	-2.575	4.884	**H**	6.729	-1.922	0.582

	x	y	z		x	y	z
H	2.101	-2.531	5.070	**O**	2.633	0.046	0.129
C	0.082	-4.235	-3.509	**N**	1.426	-2.342	-0.596
C	-0.582	-3.206	-4.439	**O**	-0.090	-0.080	-0.059
H	-0.700	-4.852	-3.033	**H**	-1.686	-3.450	-1.274
H	0.697	-4.929	-4.104	**H**	4.662	-3.278	-0.741
H	-1.214	-2.507	-3.869	**O**	1.101	0.031	2.410
H	-1.213	-3.703	-5.193	**Re**	1.246	-0.678	0.847
H	0.177	-2.606	-4.966	**H**	8.055	-2.954	1.185
C	3.340	-4.157	-3.229	**H**	-5.329	-3.080	-0.056
C	4.122	-3.107	-4.035	**H**	4.879	-3.586	-4.676
H	2.862	-4.871	-3.919	**H**	4.637	-2.396	-3.369
H	4.047	-4.751	-2.622	**C**	4.648	-3.383	4.641
H	3.446	-2.523	-4.678				

10.2 Calculation of the IRRA spectrum

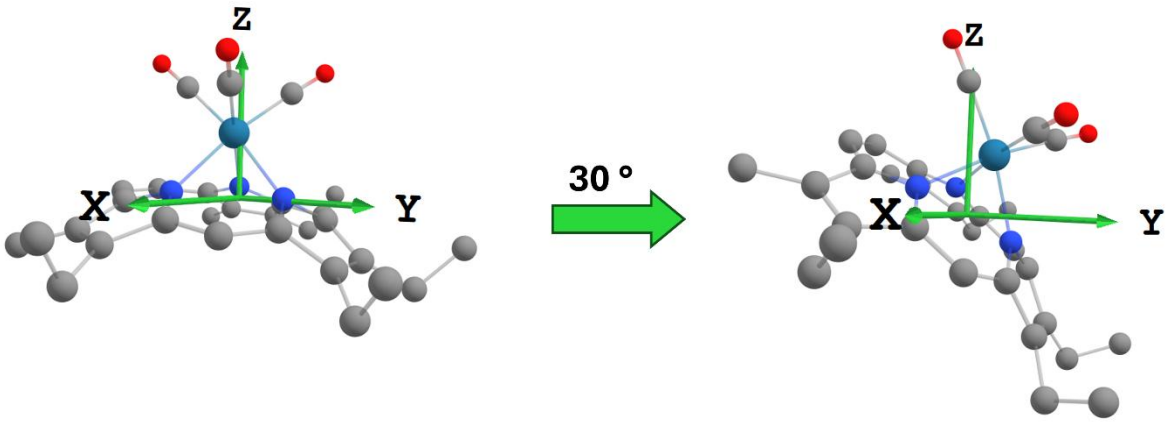

Figure S35. Initial DFT calculated structure of [Re(TriP^{Et})(CO)$_3$] (**2**) oriented parallel to the xy-plane. A tilted adsorption geometry was subsequently generated by rotating the molecule relative to this plane for the DFT simulations.

For the simulation of the IRRA spectrum a vibrational frequency DFT calculation for an isolated molecule in the gas phase was performed. Due to the surface selection rule of IRRA spectroscopy, only vibrational modes possessing a transition dipole moment (TDM) component perpendicular to the surface contribute significantly to the spectrum, while modes polarized parallel to the surface are effectively suppressed. Conventionally, the calculated total intensity (I_{sum}) of a vibrational mode arises from the vector components of its transition dipole moment along the three Cartesian axes (Equation 1). For comparison with experimental IRRA spectra, only the component perpendicular to the surface should be considered (Equation 2). In this coordinate

system, the metal substrate is defined within the xy plane, and the surface normal corresponds to the z axis.

$$I_{sum} = TDM_x^2 + TDM_y^2 + TDM_z^2 \quad (1)$$

$$I_{IRRAS} = TDM_z^2 \quad (2)$$

To achieve meaningful agreement between simulated and experimental IRRA spectra a reasonable adsorption geometry is required. Accordingly, the molecular structure was then reoriented in three-dimensional space prior to the frequency calculation to approximate its expected alignment on the surface.

References

1 M. D. Hanwell, D. E. Curtis, D. C. Lonie, Vandermeersch, T., Zurek, E., G. R. Hutchison, M. D. Hanwell, D. E. Curtis, D. C. Lonie, T. Vandermeersch, E. Zurek and G. R. Hutchison, *J. Cheminf.*, 2012, **4**, 1–17.

2 A. K. Rappe/C. J. Casewit/K. S. Colwell/W. A. Goddard III/W. M. Skiff, A. K. Rappe, C. J. Casewit, K. S. Colwell, W. A. Goddard and W. M. Skiff, *J. Am. Chem. Soc.*, 1992, **114**, 10024–10035.

3 F. Neese, *WIREs Comput Mol Sci*, 2018, **8**.

4 A. D. Becke, *The Journal of chemical physics*, 1993, **98**, 5648–5652.

5 F. Weigend and R. Ahlrichs, *Physical chemistry chemical physics : PCCP*, 2005, **7**, 3297–3305.

6 S. Grimme, J. Antony, S. Ehrlich and H. Krieg, *The Journal of chemical physics*, 2010, **132**, 154104.

7 S. Grimme, S. Ehrlich and L. Goerigk, *Journal of computational chemistry*, 2011, **32**, 1456–1465.

8 F. Neese, F. Wennmohs, A. Hansen and U. Becker, *Chemical Physics*, 2009, **356**, 98–109.

9 F. Weigend, *Physical chemistry chemical physics : PCCP*, 2006, **8**, 1057–1065.

10 G. M. Sheldrick, *Acta crystallographica. Section A, Foundations and advances*, 2015, **71**, 3–8.

11 G. M. Sheldrick, *Acta crystallographica. Section C, Structural chemistry*, 2015, **71**, 3–8.

12 H. Uno, K.-I. Nakamoto, K. Kuroki, A. Fujimoto and N. Ono, *Chem. Eur. J*, 2007, **13**, 5773–5784.

13 H. Jin, C. Gu, Z. Xiao, Q. Tan, L. Liu, L.-B. Han, W.-H. Chen and T. Chen, *Eur J Org Chem*, 2023, **26**.

14 B. Huszár, Z. Mucsi and G. Keglevich, *Molecules (Basel, Switzerland)*, 2025, **30**.

15 T. Kuga, Y. Sasano and Y. Iwabuchi, *Chem. Commun.*, 2018, **54**, 798–801.

16 D. Kuzuhara, H. Yamada, Z. Xue, T. Okujima, S. Mori, Z. Shen and H. Uno, *Chem. Commun.*, 2011, **47**, 722–724.

17 A. Schlimm, N. Stucke, B. M. Flöser, T. Rusch, J. Krahmer, C. Näther, T. Strunskus, O. M. Magnussen and F. Tuczek, *Chem. Eur. J.*, 2018, **24**, 10732–10744.

18 F. Petersen, I. Lautenschläger, A. Schlimm, B. M. Flöser, H. Jacob, R. Amirbeigiarab, T. R. Rusch, T. Strunskus, O. Magnussen and F. Tuczek, *Dalton Trans.*, 2021, **50**, 1042–1052.

19 K. U. Clausen, A. Schlimm, K. Bedbur, C. Näther, T. Strunskus, L. Fu, M. Gruber, R. Berndt and F. Tuczek, *Chem. Eur. J.*, 2024, **30**, e202303912.

20 K. U. Clausen, X. Meng, K. Reisig, C. Näther, T. Strunskus, R. Berndt and F. Tuczek, *Dalton Trans.*, 2024, **53**, 18304–18312.

21 F. Tuczek, K. Yildiz, K. U. Clausen, C. Näther and T. Strunskus, *ChemPlusChem*, 2025, e202500274.

22 G. D'Alfonso, D. Roberto, R. Ugo, C. L. Bianchi and A. Sironi, *Organometallics*, 2000, **19**, 2564–2572.

23 M. T. Greiner, T. C. R. Rocha, B. Johnson, A. Klyushin, A. Knop-Gericke and R. Schlögl, *Zeitschrift für Physikalische Chemie*, 2014, **228**, 521–541.

24 D. A. Popov, J. M. Luna, N. M. Orchanian, R. Haiges, C. A. Downes and S. C. Marinescu, *Dalton Trans.*, 2018, **47**, 17450–17460.

25 M. L. Nguyen, K. Yildiz, N. Michaelis, K. U. Clausen, T. Strunskus, C. Näther and F. Tuczek, *Z. Anorg. Allg. Chem.*, 2025, **651**, e202500143.

26 J. P. Macquet, M. M. Millard and T. Theophanides, *J. Am. Chem. Soc.*, 1978, **100**, 4741–4746.

27 D. H. Karweik and N. Winograd, *Inorg. Chem.*, 1976, **15**, 2336–2342.

28 X. Meng, M. L. Nguyen, A. Weismann, C. Li, F. Tuczek and R. Berndt, *J. Phys. Chem. C*, 2023, **127**, 12118–12124.

29 M. Angaroni, G. A. Ardizzoia, G. D'Alfonso, G. La Monica, N. Masciocchi and M. Moret, *J. Chem. Soc., Dalton Trans.*, 1990, 1895.

30 S. Watcharinyanon, C. Puglia, E. Göthelid, J.-E. Bäckvall, E. Moons and L. S. Johansson, *Surf. Sci.*, 2009, **603**, 1026–1033.

31 N. Schmidt, R. Fink and W. Hieringer, *J. Chem. Phys.*, 2010, **133**, 54703.

32 T. Okajima, Y. Yamamoto, Y. Ouchi and K. Seki, *J. Electron. Spectrosc. Relat. Phenom.*, 2001, **114-116**, 849–854.